Geophys. J. Int. (2008) **172,** 995–1015 doi: 10.1111/j.1365-246X.2007.03674.x

Far-field tsunami hazard from mega-thrust earthquakes in the Indian Ocean

Emile A. Okal[1] and Costas E. Synolakis[2,3]

[1] *Department of Earth and Planetary Sciences, Northwestern University, Evanston,* IL 60208*, USA. E-mail: emile@earth.northwestern.edu*
[2] *Department of Civil Engineering, University of Southern California, Los Angeles,* CA 90089*, USA*
[3] *Technical University of Crete,* GR-73100 *Chanea, Greece*

Accepted 2007 October 31. Received 2007 October 6; in original form 2007 March 26

SUMMARY

We evaluate far-field tsunami hazard in the Indian Ocean Basin based on hydrodynamic simulations of ten case studies of possible mega earthquakes at the major seismic zones surrounding the basin. They represent worst-case scenarios of seismic rupture along the full extent of seismogenic faults having supported large earthquakes in the historical record. In a series of numerical experiments in which the source parameters of the 2004 Sumatra tsunami are allowed to vary one by one, while keeping the seismic moment and the fault orientation unchanged, we document that the main patterns of far-field tsunami amplitudes are remarkably robust with respect to nominal variations in such parameters as hypocentral depth, exact centroid location, and slip distribution on the fault plane. These results validate the concept of modelling case scenarios of potential future earthquakes whose source is by definition imprecise.

We consider seismic sources located at the extremities of the 2004 Sumatra–Andaman rupture, namely along the southern coast of Sumatra and in the Andaman–Myanmar province; along the Makran coast of Pakistan and Iran; and also along the southern coast of Java, where the possibility of a large interplate thrust earthquake cannot be entirely dismissed. The results of our hydrodynamic simulations indicate that the distribution of maximum amplitudes in the Indian Ocean Basin is primarily controlled by the classical effect of source directivity, and additionally by refraction and focusing along bathymetric features. As a result, many provinces in the basin could be threatened by higher tsunami amplitudes than in 2004. This pattern is particularly important along the coast of East Africa, from Somalia to and including South Africa, in Madagascar and the Mascarene Islands, especially under a South Sumatra scenario involving an earthquake comparable to, or even possibly larger than, the 1833 event, whose epicentral area is widely believed to be under enhanced seismic risk as a result of stress transfer from the 2004 and 2005 ruptures to the northwest, possibly even in the wake of the 2007 Bengkulu earthquakes.

Key words: Numerical approximations and analysis; Tsunamis; Indian Ocean.

1 INTRODUCTION

The great Sumatra–Andaman tsunami of 2004 has awakened the attention of the scientific community to tsunami hazard in the Indian Ocean Basin. While regional tsunamis had been documented, for example, in Java in 1994 (Tsuji *et al.* 1995) and along the Makran coast of Pakistan * in 1945 (Byrne *et al.* 1992), the devastation wrought by the 2004 tsunami in the far field (e.g. in India, Sri Lanka, the Maldives and Somalia) was without equivalent in the historical record, and as such unexpected. Indeed, the only verifiable reports of damage from transoceanic tsunamis generated by pre-2004 earthquakes in the Indian Ocean involved the impact of the 1977 Sumbawa tsunami on the Australian coastline (Solov'ev *et al.* 1986), which at a distance of 1000 km qualifies only marginally as 'far-field', and a lone report of wave damage in the Seychelles following the 1833 tsunami in South Sumatra (Jackson *et al.* 2005). Nott & Bryant (2003) have further speculated that large boulders on the northwestern coast of Australia may have been deposited during prehistoric tsunamis, whose origin cannot be constrained. In contrast, the Car-Nicobar earthquake of 1881 December 31 generated a tsunami which was recorded in India with a maximum amplitude of only 90 cm at Nagapattinam, with apparently no mention of tsunami damage (Ortíz & Bilham 2003). These authors were also unable to verify Murty & Rafiq's (1991) claim of 5000 tsunami deaths in India following the earthquake of 1941 June 26 in the Andaman Islands.

*All names and spelling of geographical locations will reflect present-day political boundaries.

In this context, it is important to develop scenarios for future Indian Ocean mega-earthquakes which would generate transoceanic tsunamis capable of inflicting catastrophic levels of death and destruction in the far field. This paper presents hydrodynamic simulations for a number of such sources located at the subduction zones surrounding the basin.

2 METHODOLOGY

2.1 Estimation of earthquakes

Far-field tsunami hazard in an ocean basin is a direct function of the seismic potential for the extremely large events required to generate tsunamis capable of exporting death and destruction to distant shores. Our experience over the past 70 yr indicates that a seismic moment in excess of 7×10^{28} dyn $\times$ cm is required in this respect (Okal 2007a). Accordingly, we will first examine if and where the plate boundaries of the Indian Ocean basin can support such mega-earthquakes.

The 2004 Sumatra–Andaman earthquake has led scientists to a humble reassessment of the concept of a maximum expectable earthquake at a given subduction zone based on simple plate tectonics arguments. In a landmark paper, Ruff & Kanamori (1980) had proposed that the combination of the age of the subducting lithospheric plate and of the kinematic rate of convergence at the trench could be used to predict the maximum size of the relevant subduction earthquake. Under this paradigm, truly gigantic earthquakes (with a seismic moment exceeding 10^{29} dyn $\times$ cm) could occur only where young oceanic material is subducting fast into the mantle, as is the case in Chile, where the largest event ever recorded took place in 1960. By contrast, the slow subduction of a very old plate, such as at the Mariana trench, would be essentially aseismic. Based on the then available data set of plate ages and motions, Ruff and Kanamori claimed an 80 per cent correlation between maximum earthquake size and the combined physical parameters of the plate.

With a seismic moment of about 1.1×10^{30} dyn $\times$ cm (Stein & Okal 2005; Tsai *et al.* 2005), the 2004 Sumatra earthquake was the second or third largest event recorded, surpassed only by the 1960 Chilean earthquake, and perhaps by the 1964 Alaskan one. Yet, it involved lithosphere on the average 55 Myr old, subducting at no more than 5 cm yr^{-1}, which under Ruff & Kanamori's (1980) model should support only earthquakes of moment 2×10^{28} dyn $\times$ cm, capable of producing substantial tsunami damage in the near field, but insufficient to unleash a transoceanic tsunami. In the wake of the 2004 disaster, Stein & Okal (2007) recompiled both earthquake sources (including reassessed moments from historical events) and improved plate parameters (mostly convergence rates), and concluded that the resulting updated data set produced only a 30 per cent correlation between maximum size and the combined age and convergence rate of the plate, thus suggesting that a simple estimate of a 'maximum expectable earthquake' could not be reliably obtained under Ruff & Kanamori's (1980) model. Rather, we prefer to regard the length over which a fault system extends continuously along a convergent plate boundary as a *prima facie* indicator of the potential for a mega-earthquake capable of generating a tsunami destructive in the far field (Okal 2007a). Under seismic scaling laws (Geller 1976), the seismic threshold of 7×10^{28} dyn $\times$ cm translates into a minimum rupture length of 300 km, although destructive transoceanic tsunamis have occasionally been generated by shorter ruptures following earthquakes in violation of scaling laws (López & Okal 2006).

In turn, this concept brings up the delicate question of what constitutes a continuous fault zone, or conversely what can be regarded as a barrier for the propagation of rupture during a large earthquake. While it was generally accepted that major tectonic features borne by the subducting plate (e.g. a large fracture zone or a so-called 'aseismic ridge') could act as barriers, a recent reassessment of historical earthquakes in Central and Southern Peru using numerical simulations of their tsunamis in the near field (Okal *et al.* 2006a) has shown that the great 1868 Arica earthquake most probably ruptured (northwards) through the Nazca Ridge, as did the 1687 Central Peru earthquake and, at least partially, the smaller event on 2007 August 15 (both rupturing southwards).

In this context, one should also keep in mind the strong variability and unpredictability of the fragmentation of rupture during major events along a given subduction zone. In a classic study of the historical earthquakes of the Nankai trough, Ando (1975) identified four possible areas or blocks (A, B, C and D) supporting the rupture, but documented that major earthquakes occurred in an essentially random way, with the rupture involving anywhere from a single block (e.g. 'A') to two (e.g. 'C–D'), and up to all four ('A-B-C-D'), with a corresponding growth in the seismic moment and tsunami damage, the latter well documented in Japanese archives. Any incomplete, undersampled database of historical events could conceivably miss the occasional four-block earthquake and thus underestimate the maximum expectable event in the subduction zone. Ando's (1975) concept has recently been upheld in other subduction provinces, notably in Southern Chile, where it was concluded that the 1960 event had a significantly longer rupture zone than several of its 'predecessors' (Cisternas *et al.* 2005), along the Southern Kuril arc (Nanayama *et al.* 2005) and in the Pacific northwest (Kelsey *et al.* 2005).

In this general context, we identify three subduction zones, shown on Fig. 1, whose historical seismicity suggests that they bear the potential for mega-thrust events capable of generating tsunamis damaging in the far field: South Sumatra, North Andaman–Myanmar, and the Makran. We also discuss the case of South Java, where no catastrophic subduction earthquake is known in the historical record, but which could conceivably entertain one.

We wish to stress that the case studies described herein are by definition worst-case scenarios; in particular, they do not necessarily represent the next large earthquake in each of the relevant subduction zones. The latter could be smaller than envisioned in this paper, involving only one or two segments (say 'A-B') as opposed to the full fledged rupture ('A-B-C-D') in the formalism of Ando (1975). Nevertheless, we see our simulations as providing some measure of the worst possible effect of teleseismic tsunamis near distant shores; the 1960 Chilean or 2004 Sumatran earthquakes have served proof that worst-case scenarios do indeed occur.

2.2 Numerical simulations

Simulations were performed using the MOST code (Titov & Synolakis 1998), a finite-difference algorithm which solves the nonlinear shallow-water equations of hydrodynamics by the method of splitting integration steps. Full details are given in Synolakis (2002). We use a 0.1° grid (11.12 km in latitude) covering from 70°S to 28°N and from 40°E to 120°E, occasionally extended as far west as 30°W. The bathymetric grid was built from the ETOPO 2-min database of the National Geophysical Data Center, occasionally combined with individual marine charts.

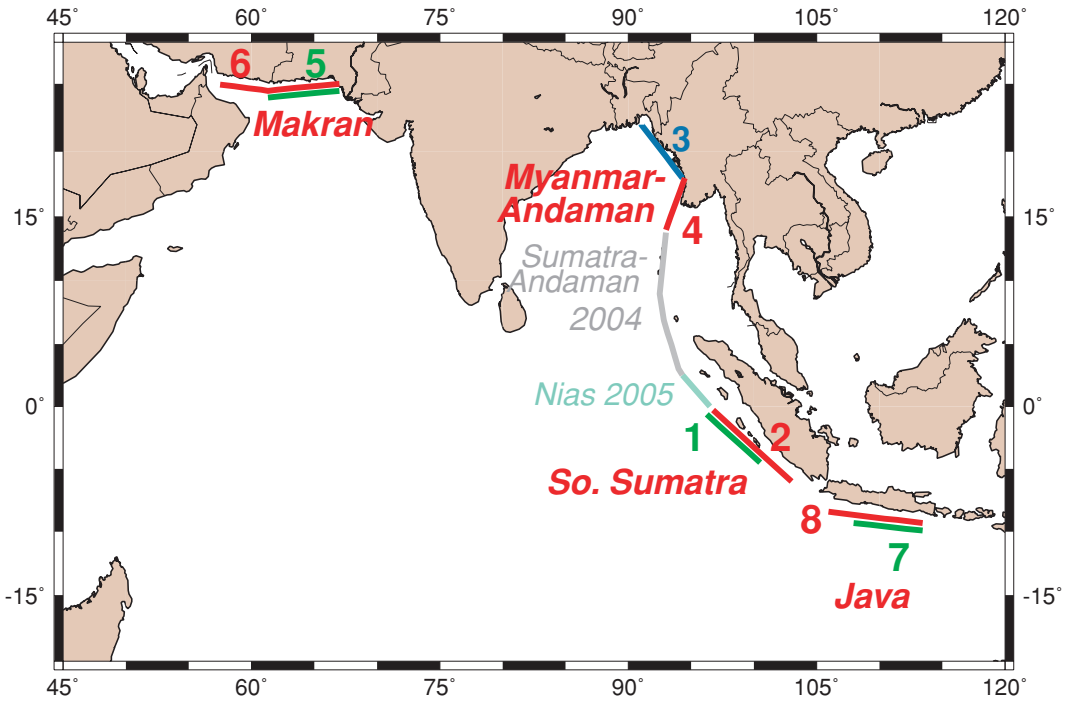

Figure 1. Map of the scenarios considered in this study. In each region, the thick traces represent the fault segments rupturing under each scenario, colour-keyed and numbered. In those regions with overlapping scenarios, the shorter fault has been offset oceanwards to enhance clarity. See text for details.

Once earthquake source parameters are selected, the static deformation resulting from the earthquake is computed using the algorithm of Mansinha & Smylie (1971), and its vertical component is then used as an initial condition of the amplitude η of the wavefield, together with a height-averaged horizontal velocity field initially set to zero. This obviously represents an approximation to the actual evolution of the seismic source, justified by the long periods of the tsunami wave, as compared to the duration of the source rupture.

The computation proceeds with a time step $\delta t = 15$ s, sufficiently short to ensure stability under the Courant–Friedrichs–Lewy conditions (Courant *et al.* 1928), even at the highest latitudes involved, where the longitudinal grid step is significantly reduced. The products of the simulations are two-fold: First, a map of the deformation of the ocean surface η is saved every 15 min (or 60 steps). In addition, a map is built of the maximum absolute amplitude reached at each grid point for the whole duration of the computation (4000 steps or 16 hr 40 mn). Note that our simulations do not include the effect of shoaling in the immediate vicinity of shorelines and of run-up on the beaches, which must be computed using site-specific high-resolution models of bathymetry and topography. Rather, they could be used as initial conditions for such local modelling at individual sites.

3 VALIDATION AND ROBUSTNESS

Before modelling possible future tsunami scenarios in the Indian Ocean basin, we validate the computational algorithm and examine its robustness relative to variations in poorly constrained earthquake parameters. For this purpose, we first consider a simplified model of the 2004 Sumatra–Andaman event, featuring a total moment $M_0 = 1.1 \times 10^{30}$ dyn $\times$ cm corresponding to a seismic slip $\Delta u = 15$ m along a fault extending north–south for $L = 1100$ km with a fault width $W = 150$ km. The focal mechanism ($\phi = 359°$; $\delta = 8°$; $\lambda = 110°$) is taken from the initial CMT solution, but the centroid of rupture is positioned at (7°N; 94°E), as suggested by the distribution of same-day aftershocks and the splitting pattern of the Earth's gravest mode, ${}_0S_2$ (Stein & Okal 2007). The top of the rupture on the fault plane is placed at a depth $h = 10$ km.

Fig. 2(e) shows the maximum amplitude simulated across the Indian Ocean Basin. We note that despite the simplified nature of the source used, the principal characteristics of the tsunami in the far field are well predicted, in particular the strong directivity of the wave towards southeastern India, Sri Lanka, the Maldives and most remarkably Somalia, where the tsunami resulted in more than 300 deaths and run-up reaching 9 m (Fritz & Borrero 2006), in contrast to the more benign effects reported at similar distances in neighbouring Kenya and Oman (Weiss & Bahlburg 2006; Okal *et al.* 2006b). As first derived by Ben-Menahem & Rosenman (1972), directivity expresses the positive interference, in the direction perpendicular to rupture, between elements of a seismic source whose rupture remains in all cases hypersonic with respect to the propagation of the tsunami.

In order to validate quantitatively the simulation, we compare it to the only available measurements of the 2004 tsunami on the high seas, namely satellite altimetry data, which featured a zero-to-peak amplitude of 70 cm on the JASON trace (Scharroo *et al.* 2005) in the vicinity of (2°N; 88°E), where we predict a maximum value of 85 cm, in good agreement with the observation. Note that a direct comparison is however impossible, since the satellite data set was neither a time nor a space series, but rather a combination obtained from a satellite cutting through the wavefield at very high speed, and as such underestimates the maximum wave amplitude at most overflown locations. In particular, the higher values (up to 1.7 m) predicted by our simulations farther north in the Bay of Bengal cannot be compared to the JASON trace, which sampled this area significantly later than the passage of the wave front carrying the maximum deformations of the sea surface.

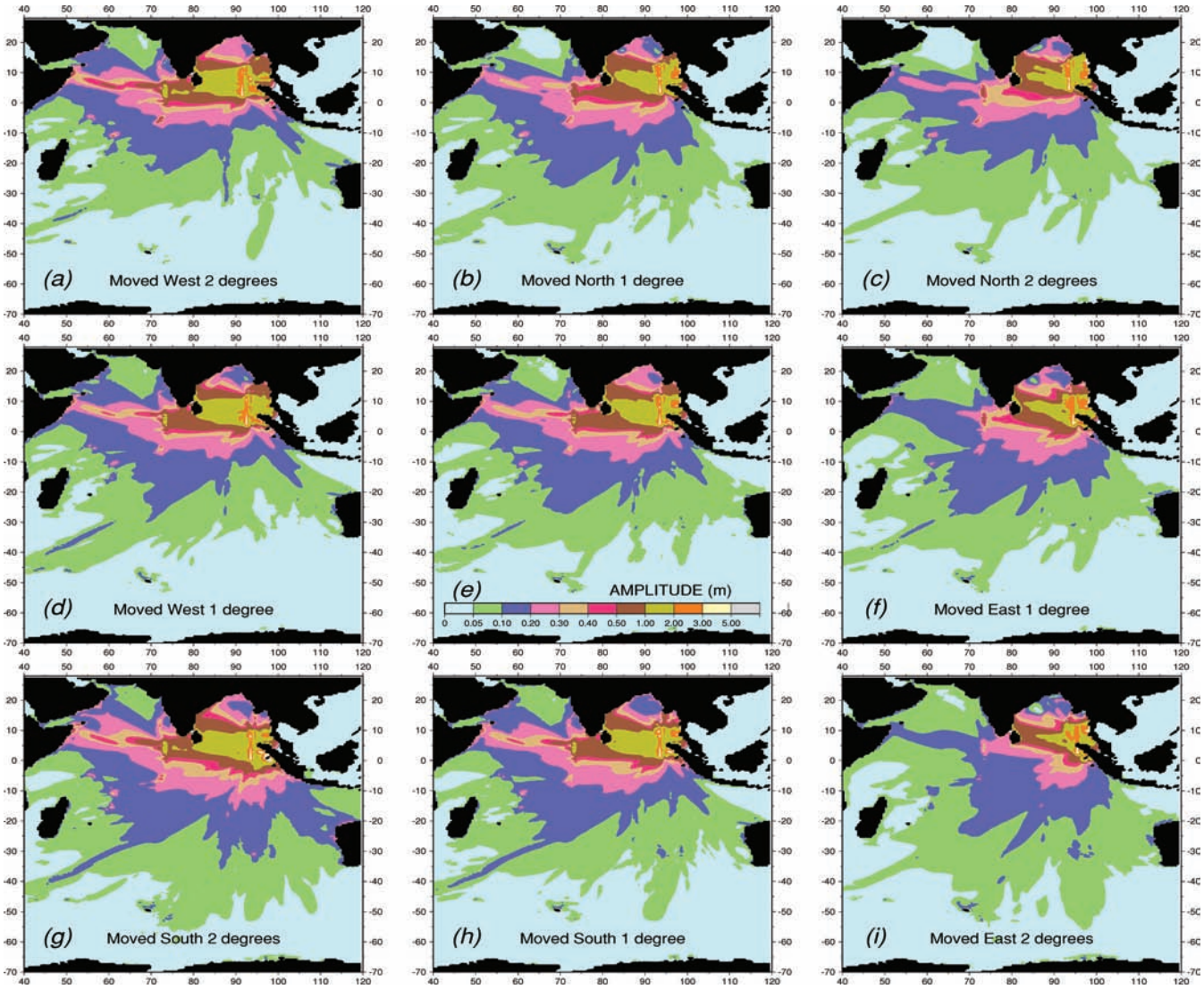

Figure 2. Robustness of simulations of the 2004 Sumatra–Andaman tsunami with respect to displacement of the parent earthquake. Each frame maps the maximum amplitude on the high seas as simulated using MOST. The central frame (*e*, with scale bar) refers to the unperturbed source, whose centroid coincides with that of the earthquake (see text for details). Frames *b*, *d*, *f*, *h*, correspond to sources displaced 1 degree in the appropriate direction (north, west, east, south, respectively). Frames displaced clockwise from each of the latter ones (*c*, *a*, *i*, *g*, respectively) correspond to a 2° displacement in the same direction. Note that with few exceptions (detailed in text), the general pattern of maximum amplitudes is conserved in all cases.

While this validation of a simulation on the high seas could be performed only against a single datum—the JASON trace, we note that similar simulations using the MOST code (Titov *et al.* 2005) have successfully predicted the recording of long-wavelength tsunami waves by coastal seismic stations, once the latter are deconvolved to represent long-wavelength tsunami amplitudes on the high seas (Okal 2007). We conclude that our simulation provides an acceptable order of magnitude of the maximum sea surface elevation, which remains poorly documented in the instrumental record.

We address the question of the robustness of the simulations by varying, one at a time, several parameters in our source model, and comparing the fields of maximum amplitude of the resulting simulations to the original one on Fig. 2(e). Such variations are taken as representative of the unavoidable uncertainties which accompany the investigation of scenarios of future earthquakes. In all cases, when one parameter of the source is varied, all other are kept unchanged.

(1) We first vary the location of the source by moving the centroid 1° (on the average 110 km) in all four directions. Frames *b*, *d*, *f*, *h* of Fig. 2 show that the far-field amplitude of the tsunami is practically unaltered, the only discernable effect being a slight decrease in amplitude due west of the event (Maldives, Somalia) when the source is moved eastwards (Fig. 2f). This is easily understood, as this displacement places most of the rupture over and beyond the Nicobar-Andaman arc into the Andaman Sea. When the translation is increased to 2°, westward and southward displacements (Figs 2a and g) have very little effect on the tsunami field, while a northward one traps more of the wavefield against India in the Bay of Bengal (Fig. 2c), allowing less illumination of the northwestern Indian Ocean Basin, in turn resulting in lower amplitudes in the Maldives and Somalia; by contrast, in the near field, the southern Coast of Myanmar is the site of enhanced amplitudes. An eastward translation of 2° further concentrates the tsunami in the Andaman Sea, from which it is funnelled into the straits of Malacca (Fig. 2i).

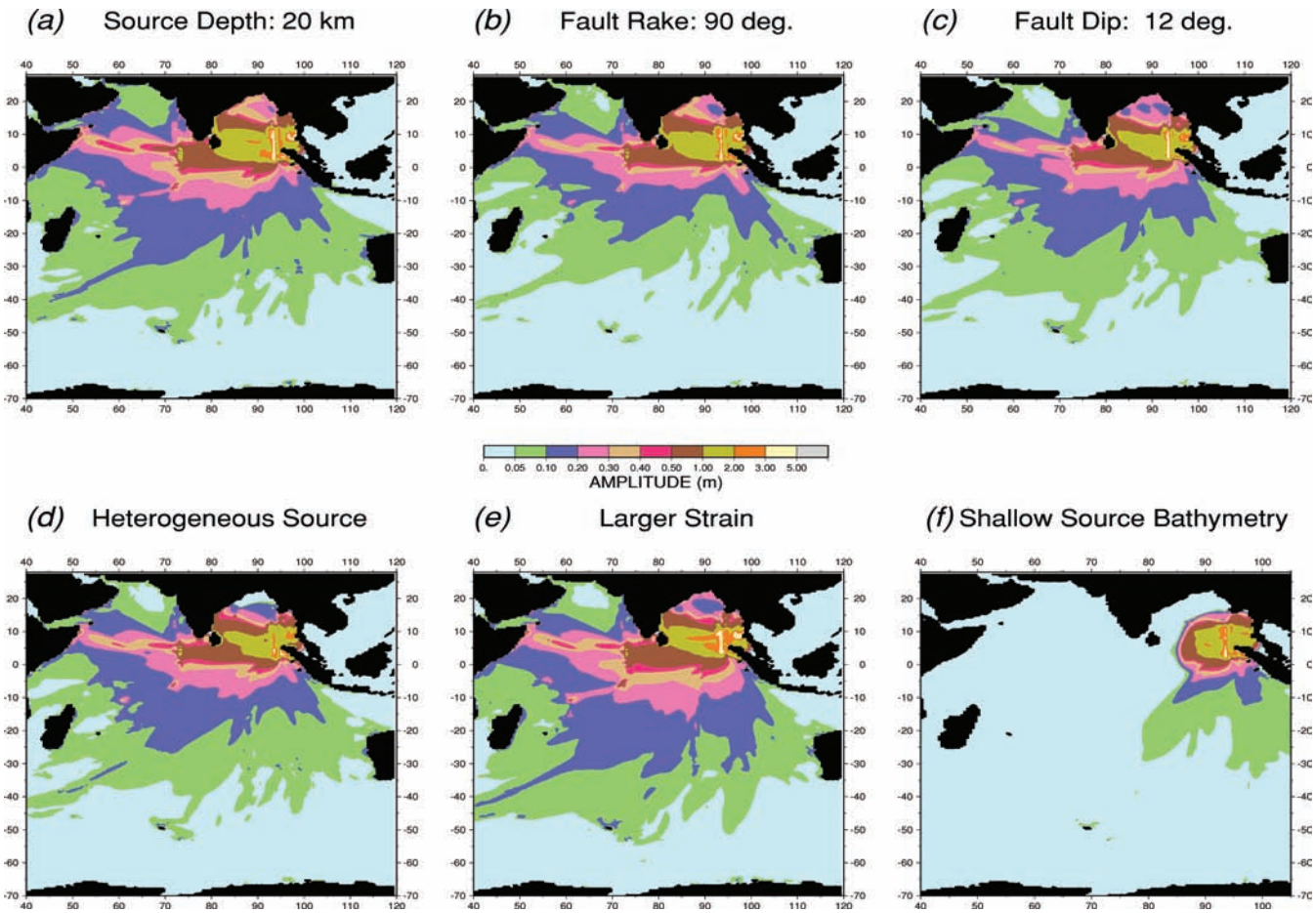

Figure 3. Robustness of simulations of the 2004 Sumatra–Andaman tsunami with respect to variations in source properties of the parent earthquake. Each frame maps the maximum amplitude on the high seas as simulated using MOST. The simulation for the unperturbed source is shown on Fig. 2(e). (a) Deeper source, stopping at a depth of 20 km. (b) Effect of change in rake. (c) Effect of change in fault dip; in this single case, the moment is adjusted to keep $M_0 \sin\delta$ constant. (d) Effect of an irregular distribution of slip on the fault plane. (e) Effect of larger seismic slip Δu on a smaller fault plane. (f) Effect of artificially reduced bathymetry in the source region; note that this is the only case for which the far field is strongly affected. See text for discussion.

The bottom line of this experiment is that, with the exception of geometrical effects due to the shape of major land structures, the exact position of a large source has only a limited effect on the large-scale properties of the tsunami in the far field.

(2) In the next experiment, we increase the source depth at the top of the earthquake rupture zone from 10 to 20 km. As shown on Fig. 3(a), the amplitude of the tsunami in the far field features only a slight *increase*, most notable along the Maldives-Somalia path. While this result may seem paradoxical, it is easily understood in the context of the representation of the tsunami as a branch of normal modes of the Earth (Ward 1980). The combination of the shallow dip and nearly pure thrust mechanism of the source approaches the geometry of a horizontal decollement which features a classical singularity of excitation at the Earth's surface (Aki & Richards 1980); sinking the source moves it away from the singularity, and thus *increases* the excitation of all seismic waves, including of the tsunami. We emphasize, however, that this effect remains minor and that the general pattern of the far field remains unaltered.

(3) We then turn to the geometry of the source, by varying the dip $\delta$and rake λ of the focal mechanism. We choose not to vary the fault strike φ, which is controlled by the plate geometry. In Fig. 3(b), we suppress the strike-slip component of the mechanism, using $\lambda = 90^\circ$; except for minor variations in its sidelobes, the far-field pattern of the tsunami is unchanged. In Fig. 3(c), we increase the dip to $\delta = 12^\circ$, while at the same time reducing the seismic moment, so as to keep constant the product $M_0 \times \sin\delta$, which controls the excitation of normal modes by shallow sources. Once again, we fail to observe any significant change in the far-field tsunami.

(4) In Fig. 3(d), we consider the case of a heterogeneous slip on the fault. While keeping the total seismic moment constant, we consider three subfaults located at the sites of the patches of maximum seismic release suggested by various studies in source tomography (e.g. Ishii *et al.* 2005; Banerjee *et al.* 2007): a first one at (3.4°N; 94.2°E) with $\Delta u = 18$ m and a moment $M_0 = 3.7 \times 10^{29}$ dyn $\times$ cm, a second one at (7°N; 94°E) with $\Delta u = 15$ m and $M_0 = 5.1 \times 10^{29}$ dyn $\times$ cm, and a third one at (10.6°N; 94.1°E) with $\Delta u = 12$ m and $M_0 = 2.5 \times 10^{29}$ dyn $\times$ cm. We find, once again, that while the introduction of such heterogeneity in the rupture may affect run-up on local beaches (Geist & Dmowska 1999), it has essentially no effect on the far-field tsunami.

(5) Next, we consider a deviation from scaling laws governing the relationship between moment M_0 and seismic slip, Δu. Specifically, we increase Δu to 20 m, while reducing the fault length L to 825 km, which leaves M_0 unchanged, but artificially increases the stress release by a factor 1.8. In the framework of Okal & Synolakis (2004), this enhances the run-up in the near field, and narrows its

distribution along a nearby beach; however, Fig. 3(e) shows that the far-field tsunami remains largely unaffected.

At this point, we can conclude that the characteristics of the tsunami in the far field appear remarkably robust with respect to perturbations in the properties of the parent earthquake, as long as the seismic moment M_0 (or in the case of a change of dip, the product $M_0 \times \sin\delta$) remains constant. This is easily understood by realizing that the far-field tsunami wave consists of an integral of the contribution of the various elements of the source, which, because of the largely linear character of the problem in the far field, is controlled primarily by the integral of the source, namely the seismic moment M_0. This situation is similar to that of seismic waves, which, in the far-field, and at long enough periods, are well described by the robust concept of a 'mantle magnitude', where measurements ignoring secondary details such as focal mechanism and depth still give rise to robust estimates of the seismic moment (Okal & Talandier 1989). This similarity is of course rooted in the representation of the tsunami as a branch of normal modes of the Earth (Ward 1980; Okal 1988), whose excitation by double couples obeys the same principles as that of seismic waves (Okal 2008). This is also reminiscent of Saint-Venant's principle in linear elasticity, which states that the detailed distribution of stress in the far field does not depend on the details of the source, but only on its total load (Knowles 1966).

The only exception to the above pattern is illustrated in our last experiment, in which we reduce substantially the thickness H of the water column over the source area. In the region extending from 90°E to 96°E and from 2°S to 15°N, we artificially divide H by 4, thus reducing the low-frequency velocity of the tsunami by a factor of 2. The area is linked to the unperturbed ocean floor by a tapered slope extending 2° on all sides. The source of the tsunami is otherwise left unchanged.

Indeed, Fig. 3(f) shows that contrary to the previous experiments, the wavefield of the tsunami is profoundly affected. The tsunami is now essentially confined to the zone of shallow bathymetry, and as such hardly exits the Bay of Bengal. The origin of this effect resides in the decrease of tsunami amplitude at the bathymetric slope between the shallow source region and the deep oceanic basin. As shown by Kajiura (1981) and confirmed under normal mode theory by Okal (2003), the total energy of an earthquake-generated tsunami does not depend on the water depth H. Nor does the initial amplitude of the ocean surface deformation η under the approximation considered in the present simulations, namely that the deformation of the ocean bottom is fully transferred to the surface. At the transition to unperturbed water depth, the wave height on the high seas will be reduced according to the classical proportionality to $H^{-1/4}$, which expresses the conservation of energy flux at the slope, and known as Green's law (Green 1837; Synolakis 1991).

This model will be valid as long as the transition takes place close enough to the source that the amplitude of the tsunami has not been dispersed by propagation. Also, we have assumed that the transition to deeper water is linear, that is, that energy flux is conserved, which will be valid only if it takes place over a distance larger than the wavelength; this may not necessarily be the case given the bathymetric taper selected, which is, however, representative of the transition slopes encountered around oceanic plateaux.

Despite these limitations, this model shows that an exceptionally shallow bathymetry in the epicentral area reduces the amplitude of the tsunami in the far field. In this respect, it confirms the experiment of Synolakis and Arcas (quoted by Kerr 2005) following the 2005 Nias earthquake. This mega-thrust earthquake ($M_0 = 1.05 \times 10^{29}$ dyn × cm) resulted in a damaging local tsunami (McAdoo *et al.* 2006), which failed to propagate in the far field. Synolakis and Arcas were able to simulate a much stronger tsunami in the far field by suppressing a number of shallow bathymetric features from the epicentral area, and replacing them with deep water. Note in particular that the rupture area of the Nias earthquake included the ultimate shallow bathymetry, namely the large islands of Simeulue and Nias, where the earthquake dislocation displaces rock rather than water, obviously lessening the amplitude of the resulting tsunami.

In conclusion, our experiments demonstrate the robustness of our simulations with respect to variations in source parameters which are expected to be typical of the uncertainties associated with constructing scenarios of future earthquakes.

4 INDIVIDUAL CASE SCENARIOS

4.1 South Sumatra

This subduction segment is located immediately to the southeast of the 2005 rupture, and extends approximately 1000 km to the Sunda Straits. It constitutes a zone of particular concern, since it is widely perceived as presently undergoing enhanced stress resulting from Coulomb stress transfer from the 2004 Sumatra–Andaman earthquake. We recall that under this model, the rupture of a segment of fault during a major earthquake results in an alteration of the regional field of stress, in particular along neighbouring segments of the fault, which may thus reach a sufficiently enhanced stress regime to themselves be triggered into rupture. When applied to the subsequent segments of a major fault system, this concept may result in a temporal propagation of seismic activity along a plate boundary, one of the most spectacular examples being the westward migration of seismicity along the North Anatolian fault since 1939 (Stein *et al.* 1997; Parsons *et al.* 2000). Immediately following the 2004 Sumatra event, McCloskey *et al.* (2005) identified a zone of enhanced stress at the southeast extremity of its rupture, precisely where the 2005 Nias earthquake occurred a few days later. In turn, the stress released during the Nias shock has been transferred to the southeast, in the general area of the 1833 earthquake, which then became widely perceived as a likely candidate for a major event (Nalbant *et al.* 2005; Borrero *et al.* 2006a). As detailed in the Appendix, the Bengkulu earthquake of 2007 September 12 fits the model of stress transfer, although it probably failed to release all stress accumulated in the area since 1833.

In this study, we first consider as a probable scenario a simple repeat of the great earthquake of 1833 November 24 ('Scenario 1'). According to the compilation by Wichmann (1918), the 1833 event was clearly catastrophic along the southwest coast of Sumatra from Pariaman to Bengkulu, with the tsunami inflicting heavy destruction and moving boats inland. In the far field, the lone report consists of significant damage in the Seychelles (Jackson *et al.* 2005); however, given the sparse settlement at the time, and the lack of surviving archives in many of the areas concerned, the impact of the tsunami could have been strong along many of the western shores of the Indian Ocean.

In a landmark study, Zachariasen *et al.* (1999) have dated emerged coral microatolls on the islands facing the southwestern coast of Sumatra to map the coseismic uplift during the 1833 earthquake, and in turn inverted this data set into the focal geometry of the event. Their solution features a slip $\Delta u = 13$ m on a rupture zone measuring $L = 550$ km by $W = 175$ km, which translates into a moment $M_0 = 6.3 \times 10^{29}$ dyn × cm, with the focal geometry $\phi = 322°, \delta = 12°, \lambda = 90°$. This mechanism correctly predicts an initial

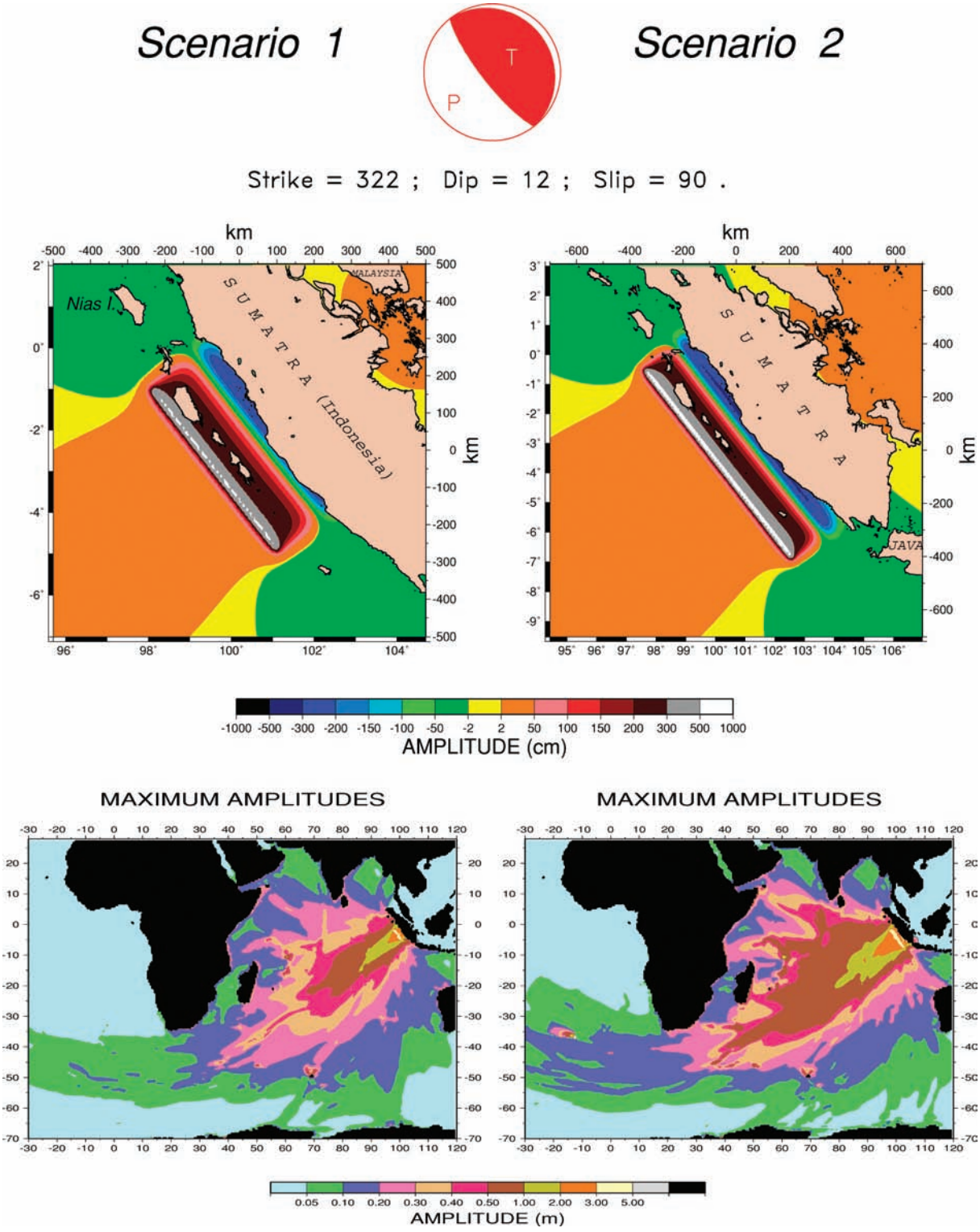

Figure 4. Simulations for Scenarios 1 (left-hand panel) and 2 (right-hand panel). The top frames show the static displacements of the parent earthquakes, which are used as initial conditions of the MOST simulations. The bottom frames map the fields of maximum amplitude of the simulations. The grid has been extended westwards to 30°W, in order to illustrate the impact of the tsunami under these scenarios on South Africa.

recess of the sea along the Sumatran coast (Tadepalli & Synolakis 1996), as described by Wichmann (1918) at Pariaman.

Simulation results for a repeat of the 1833 event under Scenario 1 are shown on Fig. 4. As expected, the difference in fault strike with the 2004 earthquake results in a directivity lobe rotated counter-clockwise, and focused on the southwestern Indian Ocean, with especially high amplitudes on Madagascar and the Mascarene Islands (Réunion, Mauritius, Rodrigues and Seychelles). In particular, we find amplitudes off the eastern coast of Madagascar about four times larger than for the 2004 model. Recalling that our computations are

stopped at the gridpoint nearest the shoreline (on the average 5 km away), and that the 2004 run-up in Madagascar ranged from 0.5 to 5 m (Okal *et al.* 2006c), we can only surmise that a repeat of the 1833 event could bring dekametric waves to the island, and hence very significant destruction to infrastructure, as well as heavy casualties.

While the tsunami is significantly less severe than the 2004 one in Sri Lanka and the Maldives, the latter act as a refracting lens focusing some energy back towards Oman, Socotra Island and Somalia, where the wave height patterns are remarkably similar to those of 2004. This should be of particular concern, given the exceptional devastation incurred by the northeastern coast of Somalia in 2004 (Fritz & Borrero 2006). The simulated tsunami seems to penetrate efficiently into the Gulf of Aden, and there is a hint that it could even reach the Red Sea. Farther south, we note that the directivity lobe of the tsunami links up with the shallow southwest Indian Ocean Ridge, itself acting as a focusing lens (Woods & Okal 1987), which results in a large beam of energy flowing into the South Atlantic, whose sidelobes bring amplitudes about 3 to 4 times greater than in the 2004 model to the southern shores of South Africa. Given reports of 2-m run-up and two drownings in South Africa during the 2004 tsunami (Synolakis & Kong 2006), any repeat of the 1833 event would be expected to pose significant hazard to that country as well.

In further assessing tsunami hazard from southern Sumatra, we note that the southeastern extremity of the 1833 rupture, as inverted by Zachariasen *et al.* (1999), is still about 350 km from the southern tip of the island at the Sunda Straits. The corresponding area bears seismicity, as evidenced by the recent interplate thrust earthquake of 2000 June 04 (4.73°S; 101.94°E; $M_0 = 7.5 \times 10^{27}$ dyn × cm), whose aftershocks extend 170 km to the southeast, and the large event of 1914 June 25, described more in detail in the Appendix. Farther to the southeast, we note an earthquake on 1950 March 27 ($M_{PAS} = 7$) and a steady level of scattered seismic activity. In the framework of Ando's (1975) observations along the Nankai trough, it may be legitimate to consider that such earthquakes represent failure on a further segment of a continuous fault zone, which may become engulfed into a future mega-thrust earthquake rupturing over and beyond the 1833 segment. In this model, the 1833 earthquake would not be the maximum one off the coast of southern Sumatra.

We therefore, consider as 'Scenario 2' an event with the same focal geometry as Scenario 1, but extending 350 km farther to the southeast, for a total length $L = 900$ km. We keep $W = 175$ km, and increase Δu to 15 m, for a total moment $M_0 = 1.13 \times 10^{30}$ dyn × cm, essentially equivalent to that of the 2004 Sumatra–Andaman earthquake. This event would be definitely larger than any one documented in the region, but so was the 2004 earthquake when it occurred. Although improbable, we have no reason to label Scenario 2 as impossible, and it must, therefore, be considered in the examination of worst-case scenarios.

Results from the simulation of Scenario 2 are shown in Fig. 4 (right-hand panel). While this study does not perform small scale modelling of inundation at individual sites, and thus no quantitative values of run-up can be quoted from our results, it is clear that offshore amplitudes are significantly increased over those of Scenario 1 and that the eventual impact on coastlines would be catastrophic at many distant locations. Among them the Maldives, Madagascar and the Mascarene Islands are particularly affected, with offshore amplitudes as high as seven times those of 2004 along the east coast of Madagascar. Similarly, our results suggest offshore amplitudes of 25 cm off South Africa, equivalent to those which attacked Somalia in 2004.

In addition, even though Australia sits well out of the lobe of directivity of the tsunami, its northwestern coast becomes significantly exposed because of the proximity of the rupture, which now extends to the vicinity of the Sunda Straits, a mere 1400 km away. Finally, and for the same reason, the tsunami penetrates the Sunda Straits.

4.2 North of Andaman, Myanmar

Just as the 2004 mega-event transferred stress to the southeast, in the general location of the 1833 earthquake, it must also have loaded the extension of its fault zone to the north. The problem in determining the geometry of any earthquake potentially resulting from this stress transfer lies in the complexity of the local tectonic regime. As summarized in Stein & Okal (2007), the 2004 Sumatra–Andaman earthquake expressed motion between the subducting Indian plate (and possibly a part of the independently moving Australian plate, and of the diffuse boundary between the two), and a platelet known as the Burma sliver, bordered on the east by the active spreading centre in the Andaman Sea (Fig. 5). It is not clear, however, how far north one can continuously extend a rigid Burma sliver: Curray *et al.* (1979) prolong it all the way to 28°N, including all of continental Myanmar west of the Sagaing fault, a model disputed by Bird (2003), who prefers to regard the portion north of 16°N as a zone of diffuse deformation (shown with question marks on Fig. 5), as suggested by background seismicity and by the incompatibility between GPS-derived motion along the Sagaing fault (Vigny *et al.* 2003) and the pole of rotation (13.9°N; 103.7°E) derived by Bird (2003) from magnetic data and seafloor morphology at the Andaman spreading Centre, near 11°N, 95°E.

In this context, and in order to define a credible scenario for a major earthquake in that province, we rely on the historical record and note Oldham's (1893) report, based on an 1841 survey by Captain Halsted, of a large event on 02 April 1762 along the coast of Bangladesh and Myanmar, from Chittagong in the north to Foul Island in the south, with uplifts of up to 4 m. Recent palaeoseismological work has confirmed the presence of emerged coral structures (Satake *et al.* 2006), of an age compatible with the 1762 earthquake (Sieh & Wang, personal communication 2006). We thus consider in Scenario 3 a model inspired by a repeat of the 1762 shock. The focal mechanism considered ($\phi = 324°$; $\delta = 20°$; $\lambda = 124°$) accounts for the probable obliquity of the motion of India relative to the orientation of the Myanmar coast. On the basis of Oldham's (1883) account, we use a fault length $L = 470$ km, a width $W = 100$ km, and a slip $\Delta u = 6.5$ m, corresponding to a total moment $M_0 = 1.5 \times 10^{29}$ dyn × cm.

On the other hand, no large earthquakes are documented, even in the historical record, along the northern extension of the 2004 rupture, between Great Coco Island and the southwestern tip of Myanmar, forming the western end of the mouths of the Irrawady. Stein & Okal (2007) have derived a pole of rotation of India with respect to the Burma sliver at 17°N; 95°E, with a rate of 2.17° Myr^{-1}. The proximity of this pole to the presumed plate boundary (distant no more than 200 km) suggests little strain accumulation, and may indeed be the primary factor having controlled the termination of the 2004 rupture. Note that these conclusions could be altered if, as is most probable, the Burma sliver is non-rigid. In this context, we include as a somewhat far-fetched but nevertheless feasible 'Scenario 4', a source featuring a slip $\Delta u = 7$ m along a fault measuring $L = 470$ km by $W = 175$ km, corresponding to a moment $M_0 = 2.8 \times 10^{29}$ dyn × cm, the geometry of faulting being $\phi = 20°$;

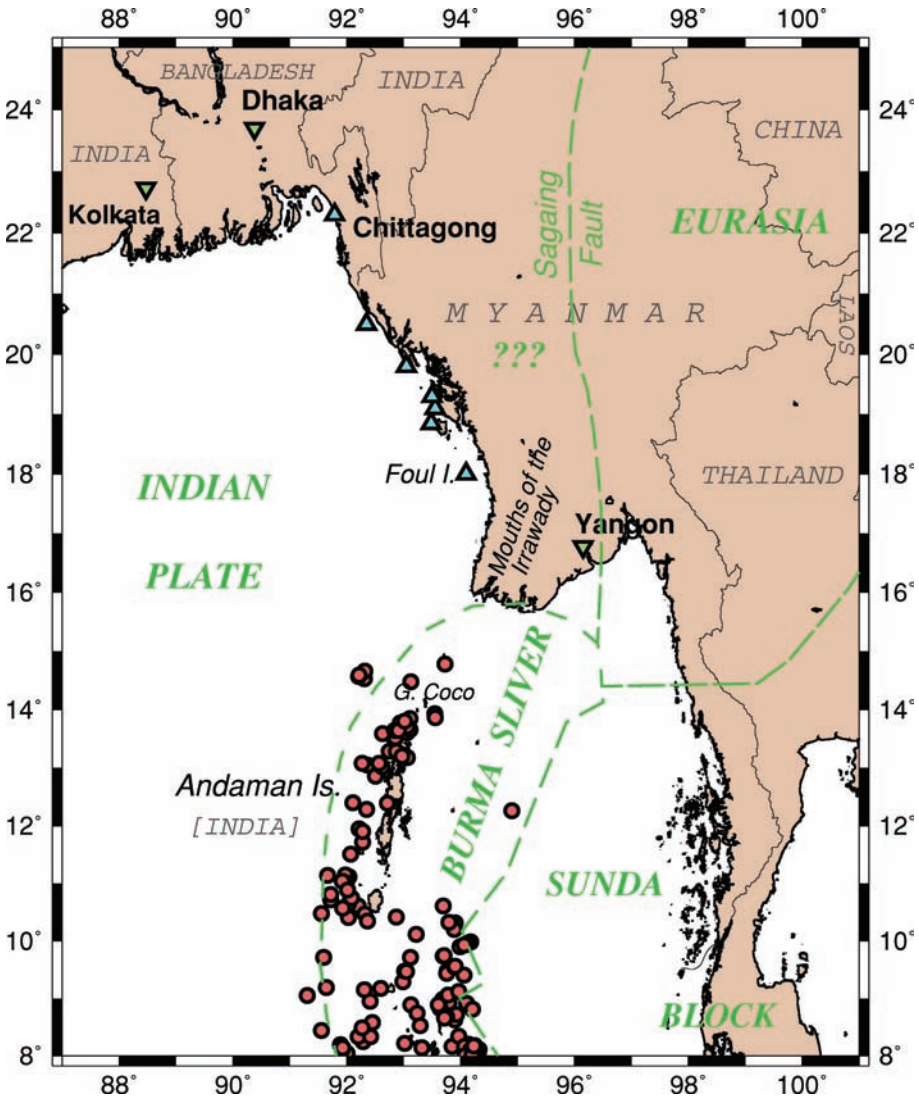

Figure 5. Seismotectonic context of the eastern shore of the Bay of Bengal. Plate boundaries are shown in green, using the model of Bird (2003), in which the Burma Sliver is limited at 16°N, the west Burmese block (shown as ???) being a zone of diffuse deformation. The red dots show the aftershocks and triggered seismicity following the 2004 Sumatra–Andaman earthquake, whose activity ceases at 14.5°N. The upwards triangles are loci of uplift during the 1762 earthquake, as compiled by Oldham (1893); the inverted ones are sites of anomalous wave activity in harbours and rivers, attributable to its tsunami.

$\delta = 15°$; $\lambda = 90°$. Note that this event is large, but its size should be considered in the context of the 2004 event, of which it could be considered as a 'left-over'. Note in particular that the seismic slip is much smaller than in Scenarios 1 or 2.

Results from simulations of Scenarios 3 and 4 are shown on Fig. 6. Both tsunamis penetrate the Indian Ocean Basin only marginally outside the Bay of Bengal. Because of the generally shallower source bathymetry for Scenario 3, the amplitude falters quicker inside the Bay than under Scenario 4, and its maximum impact, on Southern India and Sri Lanka, is less powerful than under Scenario 4 in West Bengal and Orissa. However, in both instances, substantial damage would occur along the coasts of Eastern India. Also, in both cases, and especially under Scenario 4, significant energy is funnelled into the straits of Malacca, where despite the very shallow bathymetry, it keeps decimetric amplitudes in the open sea, all the way to, and possibly beyond, Singapore, warranting a detailed inundation study to assess the impact of the tsunami on coastal infrastructure.

4.3 Makran

The Makran Coast of Baluchistan constitutes a subduction zone along which the Arabian plate sinks under the Eurasian one (Fig. 7). It was the site of a major earthquake on 1945 November 27, which was accompanied by a significant regional tsunami, with run-up in the 5–10 m range (Ambraseys & Melville 1982). Its source was studied by Byrne *et al.* (1992), who modelled it as a pure shallow-dipping underthrusting mechanism ($\phi = 236°$; $\delta = 7°$; $\lambda = 90°$; $M_0 = 1.8 \times 10^{28}$ dyn × cm). The event caused considerable damage and more than 300 deaths along the very sparsely populated Makran coast, but the relative effects of the earthquake and of the tsunami remain unclear. In the far field, the tsunami was recorded (but apparently did no damage) in the Seychelles (Beer & Stagg 1946). The complexity of the reports regarding the 1945 tsunami, in particular the occurrence of several waves separated by 2 hr, as well as the rupturing of the Mumbai–London telegraphic cable suggest that the earthquake may have triggered a delayed underwater landslide (Ambraseys & Melville 1982).

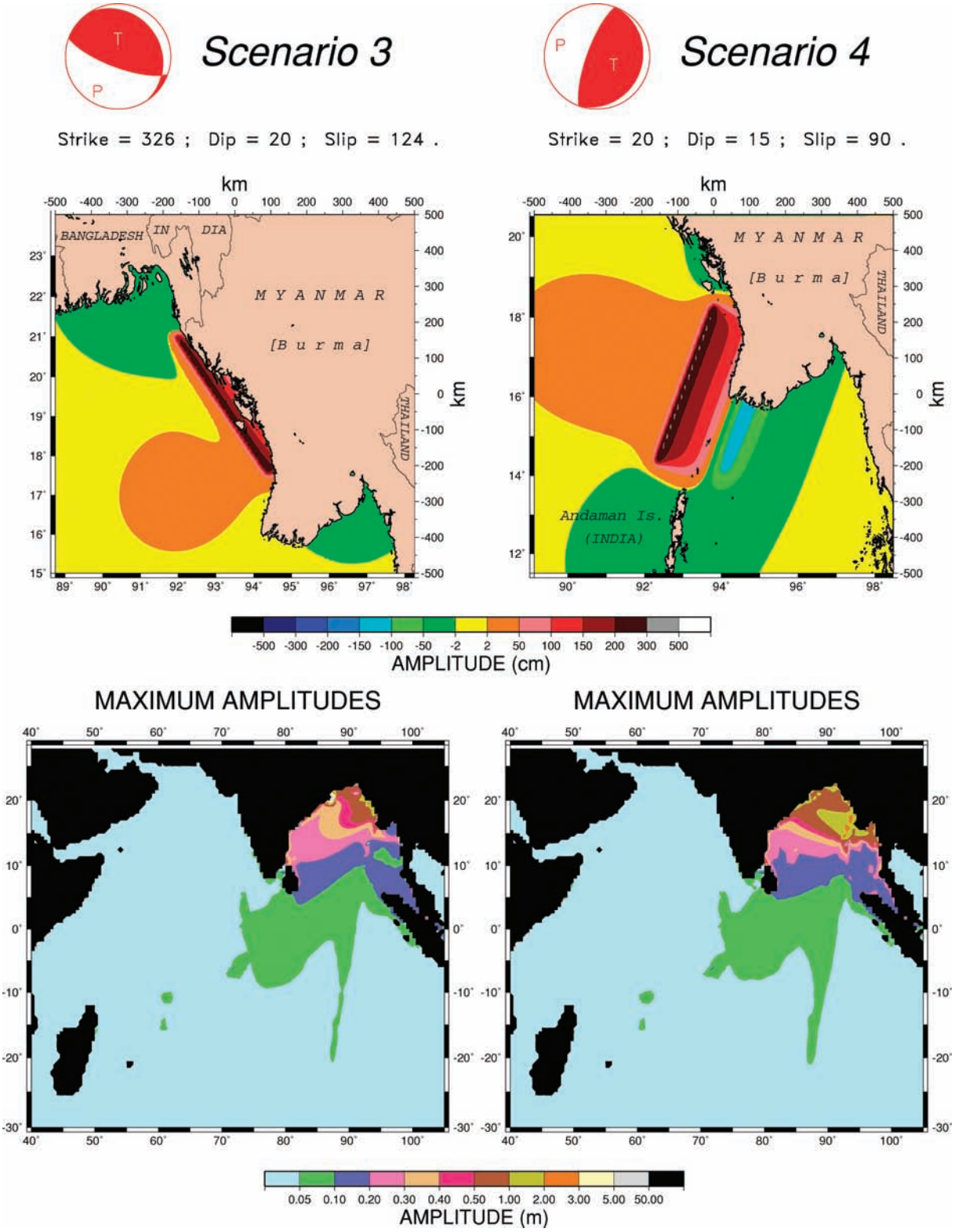

Figure 6. Same as Fig. 4 for Scenarios 3 (left-hand panel) and 4 (right-hand panel). Note that the tsunamis are largely contained to the Bay of Bengal, but are efficiently channelled into the Straits of Malacca, threatening Singapore.

A number of presumably large historical earthquakes have been documented along the Makran coast. As shown on Fig. 7, Quittmeyer & Jacob (1979) list four possibly major earthquakes, from west to east on 1483 February 18, 1851 April 19, 1864 July [August?] 25, and [about] 1765 (note that these authors regroup the 1851 and 1864 events into a single rupture in their Fig. 6). The data regarding the location and size of these shocks are extremely scant. The 1851 event is not mentioned in Ambraseys & Melville's (1982) authoritative

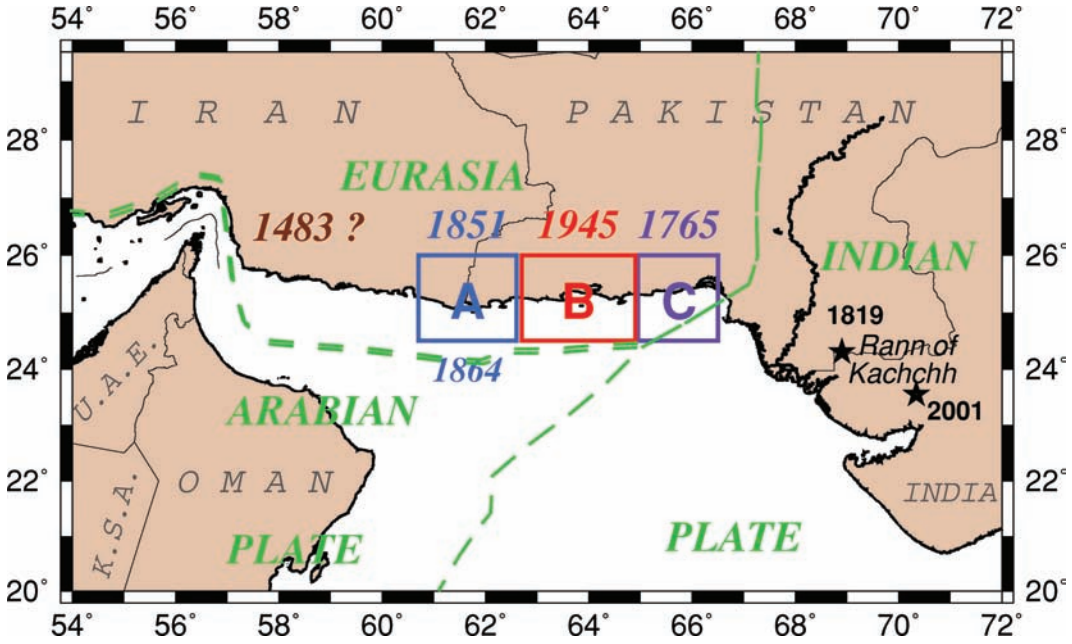

Figure 7. Map of the Makran coast of Pakistan and Iran, after Byrne *et al.* (1992). The three blocks labelled 'A', 'B' and 'C' sketch the probable rupture areas of the earthquakes of 1851 (1864), 1945 and 1765. Scenario 5 (see Fig. 8) envisions the simultaneous rupture of the three blocks, while Scenario 6 includes a western segment which could have ruptured in 1483. To the east, the stars show the epicentres of the intraplate events of 2001 and 1819, which did not generate tsunamis in the ocean.

compilation of Iranian earthquakes, even though it is located farther west, and thus closer to Iran, than the 1945 and 1765 events listed by these authors; the 1864 event is mentioned only as a note to the entry for the 1945 shock. Oldham (1893) mentions both events, his terse descriptions suggesting that the 1864 one may have been the larger. The earthquake of *ca.* 1765 precipitated a hill into the sea (Ambraseys & Melville 1982). Note finally that these events may have extremely long recurrence times, as only one earthquake of comparable size (or a doublet in the case of 1851–1864) is documented along its relevant segment of coast in the various catalogues. As for the earthquake of 1483, it is described as inflicting major damage to the region of the straits of Hormuz, with reports of a destructive earthquake in Oman at about the same period, hinting at an epicentre in or near the Gulf of Oman (Ambraseys & Melville 1982).

The picture emerging from this general framework and from a study of background seismicity (Byrne *et al.* 1992) is that of a seismogenic subduction zone in East Makran, corresponding roughly to the present shoreline of Pakistan, from about 61°E to the Indian–Arabian–Eurasian triple junction, at 67°E. To the west of 61°E (mostly along the Iranian coast), seismicity moves largely onshore, even though a deep oceanic basin is present up to 57.5°E. West of the straits of Hormuz, the convergence regime changes from oceanic subduction to continental collision, expressed by intense orogeny and seismicity in the Zagros mountains of Iran. The absence of seismicity off the coast of west Makran (57°E to 61°E) was confirmed at the microearthquake level during a short OBS deployment by Niazi *et al.* (1980). The active sediment deformation in this area was compared by White & Klitgord (1976) to that off the Oregon–Washington coast (Silver 1972), an area then regarded as featuring aseismic subduction, but where recent investigations have identified repeated, if rare, megathrust events in the palaeoseismic record (Satake *et al.* 1996; Kelsey *et al.* 2005). Thus, it is not impossible that the 1483 earthquake may have represented a rare episode of oceanic subduction in the western Makran.

In this context, we consider two scenarios for simulation. The first one, Scenario 5, inspired by Ando's (1975) paradigm, considers the simultaneous rupture of the 1851–1864 ('A'), 1945 ('B') and 1765 ('C') fault zones, as shown on Fig. 5, itself inspired by Fig. 6 of Byrne *et al.* (1992). The second and more speculative one, Scenario 6, adds another 450 km of rupture to include the probable 1483 fault zone. As in the case of Scenario 2 for the 1833 South Sumatra province, this second geometry is clearly an extreme worst-case scenario which, however, cannot be totally eliminated given the available evidence.

Simulation results for Scenarios 5 and 6 are presented on Fig. 8. Interestingly, the two fields of maximum amplitude are not significantly different, which expresses the trapping, inside the Gulf of Oman, of the wave generated by the additional fault segment in Scenario 6. At certain locations (e.g. the Gulf of Aden and the Red Sea), Scenario 6 delivers a smaller wavefield than Scenario 5, presumably reflecting a more complex form of destructive interference at the source. In addition to the obvious regional risk posed to the shores of Oman and western India, the far-field tsunami impacts the Maldives and the Seychelles. Because of unfavourable directivity patterns, it leaves relatively unaffected the shorelines of eastern and South Africa, and Madagascar. Under Scenario 6, decimetric waves could reach the continental shelf of western Australia.

4.4 The case of Java

Finally, we turn our attention to the Java subduction zone, extending from the Sunda Straits at 106°E to the island of Sumba at 120°E, beyond which no oceanic lithosphere is present (Fig. 9). This subduction zone is characterized by an absence of great interplate thrust earthquakes. In the instrumental period (since *ca.* 1900), the NEIC catalogue lists only six earthquakes with at least one magnitude $\geq$7, in 1903, 1921, 1937, 1977, 1994 and 2006. Prior to this, Newcomb & McCann (1987) document two large earthquakes in Java in 1867 and 1875, respectively. Based on an assessment of intensity maps and on the absence of tsunami reports (Wichmann 1918; Solov'ev

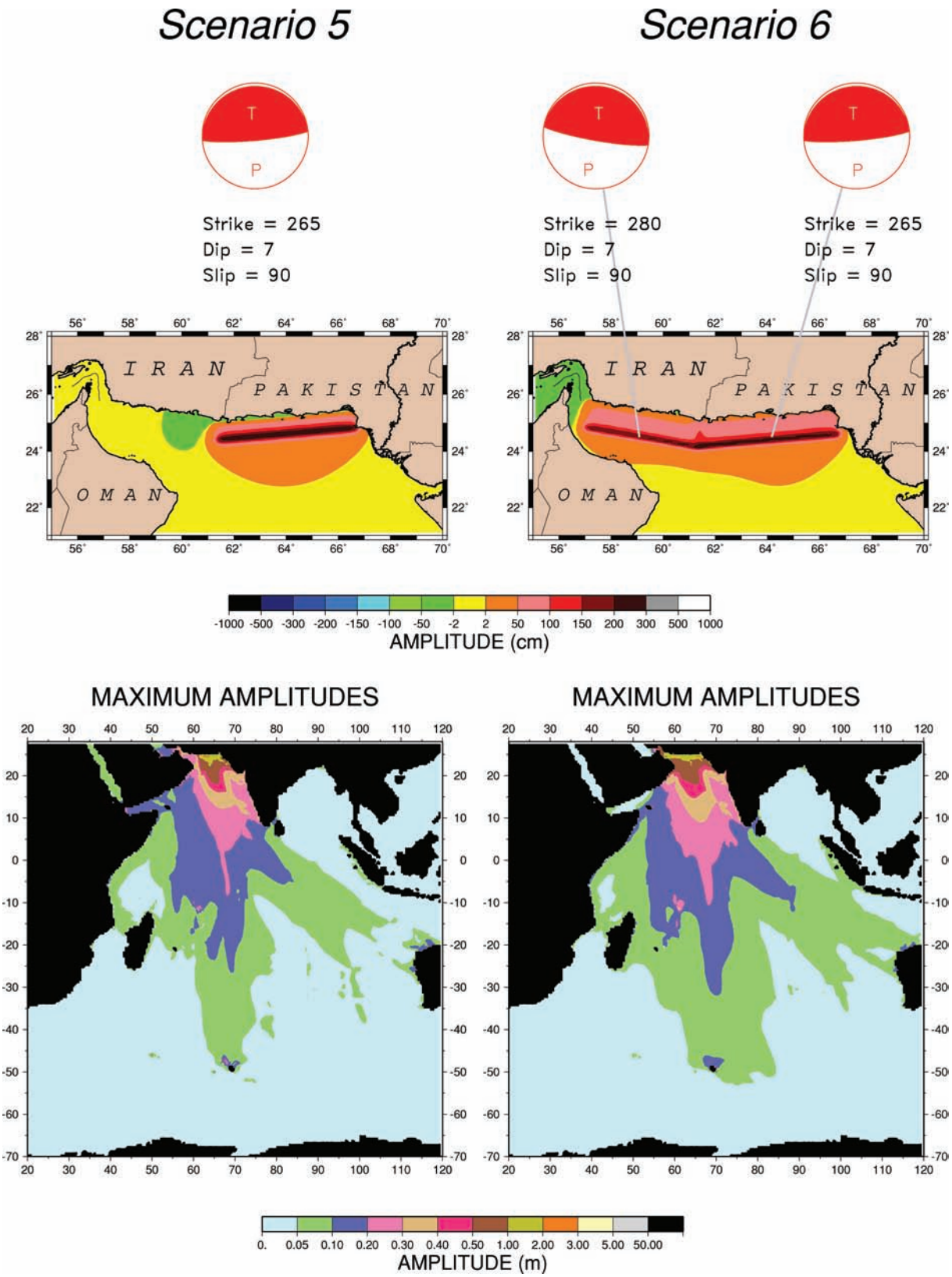

Figure 8. Same as Fig. 4 for Scenarios 5 (left-hand panel) and 6 (right-hand panel) along the Makran Coast. For the latter, the source has a composite mechanism illustrating the change of azimuth of the probable subduction zone at 61°E.

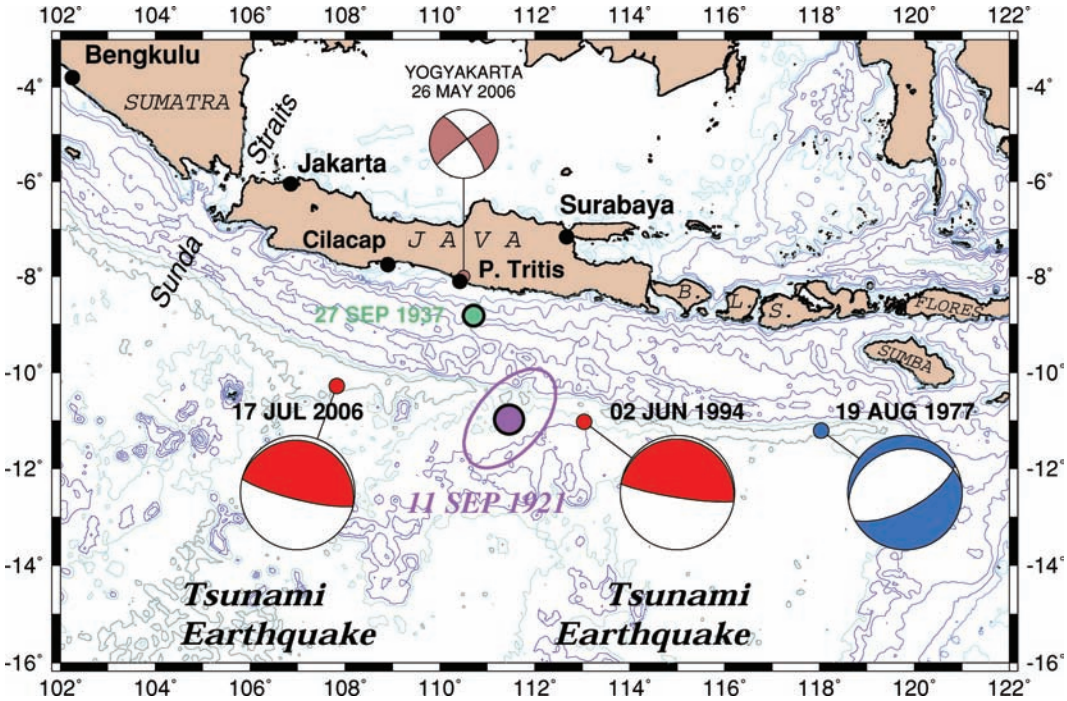

Figure 9. Map of Java and adjoining islands, with relevant major shallow earthquakes during the instrumental area. *B.*: Bali; *L.*: Lombok; *S.*: Sumbawa. Bathymetry is contoured at 1000-m intervals, with additional isobaths at 100 and 500 m. The two tsunami earthquakes of 1994 and 2006 are shown as the red beach balls, with the large 1977 Sumbawa earthquake shown in blue. For reference, the 2006 Yogyakarta earthquake is also shown (note that its epicentre was on land). Preferred relocations are shown for the 1921 earthquake (with Monte Carlo ellipse; $\sigma_G = 10$ s) and 1937 event (for the latter, the ellipse ($\sigma_G = 4$ s) is smaller than the symbol).

& Go 1984), they argued that the 1903 earthquake took place inside the western portion of the island of Java, and that the 1867 event occurred inside the island as well, being reminiscent of the more recent Yogyakarta earthquake of 2006 May 26. Similarly, there are no tsunami reports following the 1875 earthquake, which probably occurred under Java, although at an unresolvable depth. The event of 1937 September 27 ($M_{\rm PAS} = 7.2$) relocates at (8.82°S; 110.71°E), with an uncertainty ellipse of semi-major axis 25 km, but at a depth poorly constrained between 0 and 100 km. Even though this epicentre is at sea, no tsunami is mentioned. The earthquake of 1977 August 19 is a great normal faulting event ($M_0 = 3.6 \times 10^{28}$ dyn $\times$ cm) which generated a substantial local tsunami (Kato & Tsuji 1995), but no transoceanic one. The two events of 1994 June 02 and 2006 July 17 are classical 'tsunami earthquakes', defined by Kanamori (1972) as events whose tsunamis as significantly larger than expected from their magnitudes, especially conventional ones. They correspond to a rupture propagating along the fault slower than expected from seismic scaling laws (Polet & Kanamori 2000), with a resulting deficiency in high-frequency source components, as measured by the short period magnitude m_b, the radiated energy $E^{\rm E}$ (Newman & Okal 1998), or as felt by the coastal population. Indeed, along certain stretches of coastline later devastated by the tsunami, the 1994 Java earthquake was not reported felt (Synolakis *et al.* 1995; Tsuji *et al.* 1995). Because their seismic moment remains moderate (5.3 and 4.7 $\times$ 10^{27} dyn $\times$ cm, respectively), the 1994 and 2006 earthquakes did not generate transoceanic tsunamis.

The earthquake of 1921 September 11, for which Gutenberg & Richter (1954) propose $M_{\rm PAS} = 7.5$, is remarkable in many respects. It relocates at (10.98°S; 111.45°E), between the two 'tsunami earthquakes' of 1994 and 2006, and thus at a considerable distance (290 km) from the shoreline, at the oceanic trench or seaward of it (Okal & Newman 2001). On the other hand, it was felt (but produced only minor damage) over a 1500-km zone extending from Bengkulu in Sumatra to Sumbawa. Its tsunami was moderate (20 cm peak-to-peak on the maregraph at Cilacap), involving the 150-km long section of coastline from Cilacap to Parang Tritis (Visser 1922). This is in clear contrast to the two 'tsunami earthquakes' of 1994 and 2006 which were felt only marginally on the coast, but generated local tsunamis with run-up of at least 5 m along coastal segments extending more than 350 km (and reaching 21 m at one location in 2006) (Tsuji *et al.* 1995; Fritz *et al.* 2006a). We can thus rule out interpreting the 1921 event as a 'tsunami earthquake'. Rather, the most probable interpretation of its location and wide felt area would be an outer-rise intraplate normal faulting earthquake, in a geometry similar to the Sumbawa 1977 event, but on a smaller scale. Future examination of archived seismograms from the 1921 earthquake could shed additional light on this problem.

In at least two other provinces where 'tsunami earthquakes' similar to those off Java have been observed, namely Nicaragua (1992) and northern Peru (1960, 1996), the seismicity is characterized by the absence of mega-thrust earthquakes in the documented historical record, which in Peru extends back to the Spanish Conquest in 1535 (Okal & Newman 2001). It would, therefore, be tempting to regard the occurrence of 'tsunami earthquakes' and mega-thrust events as mutually exclusive, and thus to rule out the possible occurrence of the latter in Java. However, we note that the available record, extending to *ca.* 1550 (Wichmann 1918) may still undersample the seismic cycle, assuming the latter indeed exists.

In summary, the historical record of the past 150 yr fails to identify any earthquake featuring both a catastrophic level of damage and a tsunami locally devastating in Java and the neighbouring islands, which would be two required attributes for an earthquake

capable of generating a transoceanic tsunami damaging in the far field. Given the detailed nature of available catalogues (Wichmann 1918; Solov'ev & Go 1984), it is almost certain that no such event took place since 1550 A.D. However, given the possibility of very long seismic cycles, we cannot formally rule out the future occurrence of an ocean-wide tsunami generated by a mega-thrust earthquake off the coast of Java. We thus consider further two such scenarios, using the geometry of the 2006 tsunami earthquake ($\phi = 290^\circ$; $\delta = 10^\circ$; $\lambda = 102^\circ$). Scenario 7 involves a slip $\Delta u = 6$ m on a fault measuring $L = 200$ km by $W = 100$ km for a total moment of $M_0 = 5.7 \times 10^{28}$ dyn $\times$ cm; Scenario 8 envisions the full rupture of the Java segment of the subduction zone, with $L = 500$ km; $W = 150$ km; $\Delta u = 10$ m and $M_0 = 3.6 \times 10^{29}$ dyn $\times$ cm.

Simulation results for Scenarios 7 and 8 are given in Fig. 10. Scenario 7 generates deep-water amplitudes reaching 1 meter on the coast of northwest Australia (only about 1200 km from the extremity of the fault), where significant damage to infrastructure could be expected, and 25 cm at some locations along the coast of Madagascar; elsewhere in the Indian Ocean Basin, its far-field effects should be benign. By contrast, Scenario 8 would put all the coasts of northern and western Australia under deep-water amplitudes of 1–2 m, suggesting locally dekametric run-up and catastrophic inundation; an edge wave also skirts the coast of Sumatra, resulting in similar amplitudes in its southern part, and the tsunami penetrates efficiently into the Java Sea, through the straits of Sunda and Lombok. It attacks Madagascar with greater amplitudes than the 2004 Sumatra–Andaman tsunami, and also threatens the coast of South Africa.

4.5 Other sources in the Indian Ocean?

For completeness, we explore the possibility of other sources of transoceanic tsunamis in the Indian Ocean. The Southwest Indian Ocean Ridge (SWIOR) features a number of very long transform faults, including the Andrew Bain Fracture Zone (50°S; 30°E), which supported on 1942 November 10 the largest earthquake ever recorded on an oceanic transform fault ($M_0 = 1.3 \times 10^{28}$ dyn $\times$ cm) (Okal & Stein 1987). In principle, the Bain Fracture Zone extending continuously for 440 km, could support an even larger strike-slip earthquake, but because its vertical extent is thermally limited to at most 25 km, the moment of the resulting event would not exceed 5×10^{28} dyn $\times$ cm, and we have verified that its tsunami would be negligible in the far field.

The only other geological feature continuous on a sufficiently long scale to conceptually support gigantic earthquakes is the Ninetyeast Ridge, generally interpreted as a hotspot trace overprinting the large transform fault of a fossil spreading centre (Sclater & Fisher 1974; Pierce 1978). Even though this region, described as the diffuse boundary between the Indian and Australian plates (Wiens *et al.* 1986), has supported significant seismicity, the relevant moments remain below 10^{28} dyn $\times$ cm, and the earthquake mechanisms do not correspond to a precise reactivation of the Ninetyeast Ridge in its original geometry (Stein & Okal 1978). In particular, they do not use the Ridge as their fault plane, and so this seismicity does not lend itself to an extrapolation of size to tsunamigenic levels under Ando's (1975) paradigm.

Murty & Rafiq (1991) have listed as potentially tsunamigenic continental earthquakes occurring close to sea shores in the Indian subcontinent. Among such events, the largest in recent history took place in 1819 in the Rann of Kachchh (Fig. 5), and was studied extensively by Bilham (1999). The Rann, a desertic sea level depression which was navigable in medieval and earlier times, underwent coseismic flooding in 1819, described by Bilham as a tsunami, but there are no such reports in the far field, as would be expected from an earthquake with considerable seismic slip (reaching 11 m), but relatively contained dimensions (at most 150 km $\times$ 25 km), and whose moment does not exceed 5×10^{27} dyn $\times$ cm. Neither did the even smaller event in 2001 generate an oceanic tsunami, despite its catastrophic nature on land. We conclude that none of these non-subduction sources would be capable of generating a transoceanic tsunami.

5 DISCUSSION AND CONCLUSION

We have investigated the far-field amplitude of tsunamis in the Indian Ocean for a number of scenarios of mega-thrust earthquakes, ranging from probable to possible. Of those, Scenarios 1 and 3, involving the repeat of known events, are most probable, although the recent 2007 Bengkulu earthquake may have decreased both the likelihood and the size of an event under Scenario 1. Scenario 4 involves a large rupture in a zone loaded by stress transfer and otherwise known for background seismic activity. Scenarios 2, 5 and 6 represent extrapolations of the fault ruptures of known events or combinations with neighbouring segments under Ando's (1975) model. Scenarios 7 and 8 are the most speculative in that no major earthquakes are known off Java.

The most important lesson from the scenarios investigated in this study is that the patterns of far-field maximum amplitudes predicted by our simulations will not be a repeat of those observed in 2004. This specificity is the direct consequence of the directivity patterns creating a positive interference in the direction perpendicular to faulting, as derived by Ben-Menahem & Rosenman (1972), Okal & Talandier (1991) having further demonstrated that the width of directivity lobes decreases sharply with increasing earthquake size. To a lesser extent, irregular bathymetry also contributes to controlling far-field amplitudes through focusing effects (Woods & Okal 1987), as exemplified along the SWIOR, a situation already described in 2004 (Titov *et al.* 2005).

We now present a geographic description of the risk posed by distant mega-earthquakes to various coastlines of the Indian Ocean Basin.

5.1 India and Sri Lanka

To a large extent, Sri Lanka and the eastern coast of India, which had taken the onslaught of the 2004 tsunami, would suffer lesser amplitudes under the scenarios considered here. Only Scenario 4 would lead to comparable damage in the northern portion of the coast of India (principally in the state of Orissa), while Scenario 3 would affect the entire coast, but at a lower level. Scenarios 1 and 2 would probably result in significant, but not catastrophic, impact.

The western coast of India would be directly exposed in Scenarios 5 and 6 (the Makran earthquakes), with an impact obviously increasing with latitude. Historical reports of significant destruction in Mumbai in 1945 warrant immediate warning and response along the entire western coast of the country upon occurrence of any comparable or larger earthquake in the Makran.

5.2 Maldives

In the envisioned scenarios, the Maldives would be less impacted than in 2004, due primarily to different patterns of far-field directivity in the geometries involved. Thanks to the structure of the

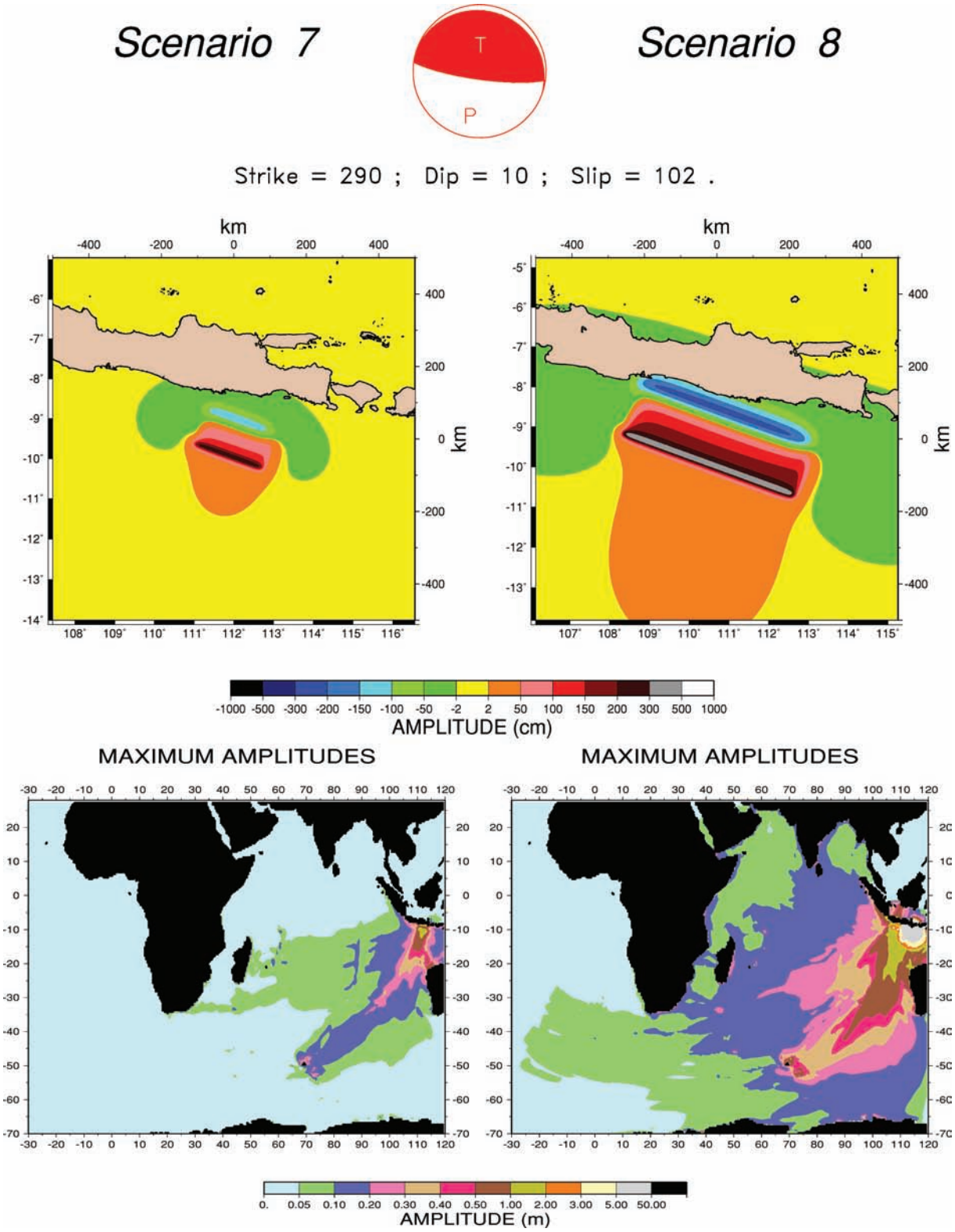

Figure 10. Same as Fig. 4 for Scenarios 7 (left-hand panel) and 8 (right-hand panel) along the coast of Java. Note the significant threat from the latter to Madagascar and South Africa.

islands (steep coral atolls with relatively narrow transverse dimensions), the tsunamis run up much less efficiently than on a typical shallow-dipping structure. Consequently, flow depths in the Maldives in 2004 were less than half the run-up values in Somalia, at half the distance from the source (Fritz *et al.* 2006b). On the other hand, the low-lying structure of the islands makes it obviously more difficult for the population to seek refuge at higher ground.

5.3 Madagascar and the Mascarenes

Because the 2004 directivity lobe was oriented at a more northerly azimuth, these islands suffered only marginally in 2004 with only one death confirmed at the southern tip of Madagascar (Okal *et al.* 2006c). By contrast, the islands would be severely attacked under Scenarios 1, 2, 7 and 8. A repeat of the 1833 event under Scenario 1 would strongly impact the Mascarenes (Seychelles, Mauritius, Rodrigues and Réunion), as expected from the historical record of damage in 1833 in the Seychelles (Jackson *et al.* 2005). The eastern coast of Madagascar, which experienced only contained flooding without significant damage in 2004, could expect destruction of coastal infrastructure with corresponding casualties under Scenario 1.

5.4 Africa

With more than 300 deaths in Somalia, 10 in Tanzania, and two in South Africa, the 2004 Sumatra–Andaman earthquake provided a rude awakening to the reality of tsunami hazard along the eastern coast of the African continent (Fritz *et al.* 2006a; Weiss & Bahlburg 2006). The principal danger for the coasts of Kenya, Tanzania and South Africa would be a repeat of the 1833 earthquake under Scenario 1, with expected impact more severe than in 2004, principally due to the more southerly azimuth of the directivity pattern. The Comoro Islands, located between Tanzania and Madagascar, would also be affected more severely than in 2004, when run-up reached 6 m on Grande Comore and 4.8 m in Mayotte (Borrero *et al.* 2006b). Significantly, and despite a less favourable directivity pattern, Somalia would remain at high risk, due to a focusing effect at the Maldives ridge.

5.5 Australia

The western coasts of Australia are at greatest risk under Scenarios 7 and 8, which could generate catastrophic levels of destruction, despite the generally sparse level of development along its coastline. It would also be threatened by a repeat of the 1833 earthquake, and especially so under Scenario 2, featuring a rupture extending to within 1400 km of the northwestern corner of the Australian continent. Significantly, the Makran Scenarios 5 and 6 can also generate tsunamis with deep-water heights comparable to those observed in 2004.

5.6 Malaysia, Singapore and northern Java

An interesting aspect of our research concerns the ability of the scenario tsunamis to penetrate straits and shallow seas, especially in the Southeast Asian area. In general, it results from a subtle trade-off between the classic amplification of the wave upon shoaling in shallow water and its inefficient propagation in extremely shallow seas. In practical terms, we find that the Straits of Malacca are sheltered by the island of Sumatra from the South Sumatra tsunamis (Scenarios 1 and 2), but directly exposed to the Myanmar events (Scenarios 3 and especially 4), which could lead to significantly more damage than in 2004 for their coastal communities, including Singapore. The northern coast of Java, with the metropoleis of Jakarta and Surabaya could be affected by diffraction of the tsunami at the Sunda Straits under Scenarios 2 or 8, and at the Bali-Lombok Straits under Scenarios 7 and 8.

5.7 Kerguelen

Finally, we consider the case of the Kerguelen Islands (49.5°S; 69.5°E), part of the Terres Australes et Antarctiques Françaises, which were emplaced in the Eocene and Oligocene on top of the Kerguelen Plateau, one of the major Large Igneous Provinces, itself formed as a flood basalt unit in the Lower Cretaceous (Frey *et al.* 2000). The presence of the plateau (prolonged as the Broken Ridge on the Australian plate) strongly affects the propagation of tsunami waves. As a result, most of our scenarios feature a substantial amplification at and near the islands, with offshore tsunami amplitudes reaching 20 cm under Scenarios 5 and 6, 40 cm under Scenario 7, and up to 1 meter under Scenarios 1, 2 and 8, as opposed to only 10 cm in 2004. Despite the extreme isolation of the islands, they host a scientific base with a population varying between 60 and 100; there are only scant reports of the effects of the 2004 tsunami on Kerguelen, where apparently it did not cause damage; however the much larger offshore amplitudes under our scenarios would clearly put the islands at risk. Future tsunamis may also have an ecological impact, as penguin rookeries were destroyed at Crozet Islands (46.4°S; 51.9°E) during the 2004 tsunami (Viera *et al.* 2006), despite offshore amplitudes not exceeding 10 cm.

ACKNOWLEDGMENTS

We thank Kerry Sieh and Yu Wang for communicating their palaeoseismic results in Myanmar prior to publication, and Seth Stein for discussion of plate kinematics. Jose Borrero shared his most recent field and modelling results regarding the Bengkulu event. Suzan van der Lee kindly helped translate original Dutch publications. This research was supported by the National Science Foundation, under grants CMS-03-01054 to EAO and CMS-03-01081 to CES, and by a 'TRANSFER' grant of the European Union to the Institute of Applied and Computational Mathematics of the Foundation of Research and Technology of Hellas (FORTH). Figures were drafted using the GMT software (Wessel & Smith 1991).

REFERENCES

Aki, K. & Richards, P.G., 1980. *Quantitative Seismology*, W.H. Freeman, San Francisco, 932 pp.

Ambraseys, N.N. & Melville, C.P., 1982. *A History of Persian Earthquakes*, Cambridge University Press, Cambridge, 219 pp.

Ando, M., 1975. Source mechanism and tectonic significance of historical earthquakes along the Nankai trough, Japan, *Tectonophysics*, **27**, 119–140.

Banerjee, P., Pollitz, F., Nagarajan, B. & Bürgmann, R., 2007. Coseismic slip distributions of the 26 December 2004 Sumatra-Andaman and 28 March 2005 Nias earthquakes from GPS static offsets, *Bull. seism. Soc. Amer.*, **97**, S86–S102.

Beer, A. & Stagg, J.M., 1946. Seismic sea-wave of November 27, 1945, *Nature*, **158**, 63–64.

Ben-Menahem, A. & Rosenman, M., 1972. Amplitude patterns of tsunami waves from submarine earthquakes, *J. geophys. Res.*, **77**, 3097–3128.

Bilham, R., 1999. Slip parameters for the Rann of Kachchh, India, 16 June 1819 earthquake, quantified from contemporary accounts, in *Coastal Tectonics*, pp. 295–318, eds Stewart, I.S. & Vita-Finzi, C., Geol. Soc. London Spec. Pub., **146**.

Bird, G.P., 2003. An updated digital model of plate boundaries, *Geochem. Geophys. Geosyst.*, **4**(3), Paper GC000252.

Borrero, J.C., Sieh, K., Chlieh, M. & Synolakis, C.E., 2006a. Tsunami inundation modeling for Western Sumatra, *Proc. Natl. Acad. Sci. USA*, **103**, 19 673–19 677.

Borrero, J.C., Fritz, H.M., Synolakis, C.E. & Okal, E.A., 2006b. Basin-wide runup measurements of the 26 December 2004 Indian Ocean tsunami, *Eos, Trans. Amer.Geophys. Un.*, **87**(52), U53C-03, [Abstract].

Borrero, J.C., Hidayat, R., Suranto, Bosserelle, C. & Okal, E.A., 2007. Field survey and preliminary modeling of the near-field tsunami from the Bengkulu earthquake of 12 September 2007, *Eos, Trans. Amer. Geophys. Un.*, **88**(52), U54A-04, 2007 [Abstract].

Byrne, D.E., Sykes, L.R. & Davis, D.M., 1992. Great thrust earthquakes and aseismic slip along the plate boundary of the Makran subduction zone, *J. geophys. Res.*, **97**, 449–478.

Chamot-Rooke, N. & Le Pichon, X., 1999. GPS-determined Eastward Sundaland motion with respect to Eurasia confirmed by earthquake slip vectors at Sundaland Philippine trenches, *Earth planet. Sci. Letts.*, **173**, 439–455.

Chlieh, M. *et al.*, 2007. Coseismic slip and after slip of the great $M_w = 9.15$ Sumatra-Andaman earthquake of 2004, *Bull. seism. Soc. Amer.*, **97**, S152–S173.

Cisternas, M. *et al.*, 2005. Predecessors of the giant 1960 Chile earthquake, *Nature*, **437**, 404–407.

Courant, R., Friedrichs, K. & Lewy, H., 1928. Über die partiellen Differenzengleichungen der mathematischen Physik, *Mathematische Annalen*, **100**, 32–74.

Curray, J.R., Moore, D.G., Lawver, L.A., Emmel, F.J., Wait, R.W., Henry, M. & Kieckhefer, R., 1979. Tectonics of the Andaman Sea in Burma, in *Geological and Geophysical Investigations of Continental Margins*, Vol. 29, pp. 189–198, Amer.Assoc. Petrol. Geol., Tulsa.

Dorbath, L., Cisternas, A. & Dorbath, C., 1990. Assessment of the size of large and great historical earthquakes in Peru, *Bull. seism. Soc. Amer.*, **80**, 551–576.

Frey, F.A. *et al.*, 2000. Origin and evolution of a submarine large igneous province: the Kerguelen Plateau and Broken Ridge, Southern Indian Ocean, *Earth planet. Sci. Letts.*, **176**, 73–89.

Fritz, H.M. & Borrero, J.C., 2006. Somalia field survey after the December 2004 Indian Ocean tsunami, *Earthq. Spectra*, **22**, S219–S233.

Fritz, H.M. *et al.*, 2006a. Survey of the July 17, 2006 Central Java tsunami reveals 21 m runup heights, *Eos, Trans. Amer. Geophys. Un.*, **87**(52), S14A-06 [Abstract].

Fritz, H.M., Synolakis, C.E. & McAdoo, B.G., 2006b. Maldives field survey after the December 2004 Indian Ocean tsunami, *Earthq. Spectra*, **22**, S137–S154.

Geist, E.L.L. & Dmowska, R., 1999. Local tsunamis and distributed slip at the source, *Pure Appl. Geophys.*, **154**, 485–512.

Geller, R.J., 1976. Scaling relations for earthquake source parameters and magnitudes, *Bull. seism. Soc. Amer.*, **66**, 1501–1523.

Green, G., 1837. On the motion of waves in a variable canal of small depth, *Cambridge Phil. Trans.*, **6**, 457–462.

Gutenberg, B. & Richter, C.F., 1954. *Seismicity of the Earth and Associated Phenomena*, Princeton University Press, Princeton, NJ.

Ishii, M., Shearer, P.M., Houston, H. & Vidale, J.E., 2005. Extent, duration and speed of the 2004 Sumatra-Andaman earthquake imaged by the Hi-net array, *Nature*, **435**, 933–936.

Jackson, L.E., Barrie, J.V., Forbes, D.L., Shaw, J., Mawson, G.K. & Schmidt, M., 2005. Effects of the 26 December 2004 Indian Ocean tsunami in the Republic of Seychelles, *Eos. Trans. Amer. Geophys. Un.*, **86**(52), F6–F7 [Abstract].

Kajiura, K., 1981. Tsunami energy in relation to parameters of the earthquake fault model, *Bull. Earthq. Res. Inst. Tokyo Univ.*, **56**, 415–440.

Kanamori, H., 1972. Mechanism of tsunami earthquakes, *Phys. Earth planet. Inter.*, **6**, 346–359.

Kato, K. & Tsuji, Y., 1995. Tsunami of the Sumbawa earthquake of August 19, 1977, *J. Nat. Disaster Sci.*, **17**, 87–100.

Kelsey, H.M., Nelson, A.R., Witter, R.C. & Hemphill-Haley, E., 2005. Tsunami history of an Oregon coastal lake reveals a 4,600-year record of great earthquakes on the Cascadia subduction zone, *Geol. Soc. Amer. Bull.*, **117**, 1009–1032.

Kerr, R.A., 2005. Model shows islands muted tsunami after latest Indonesian quake, *Science*, **308**, 341.

Knowles, J.K., 1966. On St. Venant's principle in the two-dimensional linear theory of elasticity, *Arch. Rat. Mech. Anal.*, **21**, 1–22.

López, A.M. & Okal, E.A., 2006. A seismological reassessment of the source of the 1946 Aleutian "tsunami" earthquake, *Geophys. J. Int.*, **165,** 835–849.

Mansinha, L. & Smylie, D.E., 1971. The displacement fields of inclined faults, *Bull. seism. Soc. Amer.*, **61**, 1433–1440.

McAdoo, B.G., Dengler, L., Prasetya, G. & Titov, V.V., 2006. Smong: How an oral history saved thousands on Indonesia's Simeulue Island during the December 2004 and March 2005 tsunamis, *Earthq. Spectra*, **22**, S661–S669.

McCloskey, J., Nalbant, S.S. & Steacey, S., 2005. Earthquake risk from co-seismic stress, *Nature*, **434**, 291.

Murty, T.S. & Rafiq, M., 1991. A tentative list of tsunamis in the marginal seas of the North Indian Ocean, *Nat. Haz.*, **4**, 81–83.

Nalbant, S.S., Steacey, S., Sieh, K., Natawidjaja, D. & McCloskey, J., 2005. Updated earthquake hazard in Sumatra, *Nature*, **435**, 756–757.

Nanayama, F., Satake, K., Furukawa, R., Shimokawa, K., Atwater, B.F., Shigeno, K. & Yamaki, S., 2005. Unusually large earthquakes inferred from tsunami deposits along the Kuril trench, *Nature*, **434**, 660–663.

Newcomb, K.R. & McCann, W.R., 1987. Seismic history and seismotectonics of the Sunda Arc, *J. geophys. Res.*, **92**, 421–439.

Newman, A.V. & Okal, E.A., 1998. Teleseismic estimates of radiated seismic energy: the E/M_0 discriminant for tsunami earthquakes, *J. geophys. Res.*, **103**, 26 885–26 898.

Niazi, M., Shimamura, H. & Matsu'ura, M., 1980. Micro-earthquakes and crustal structure off the Makran coast of Iran, *Geophys. Res. Letts.*, **7**, 297–300.

Nott, J. & Bryant, E., 2003. Extreme marine inundations (tsunamis?) of coastal Western Australia, *J. Geology*, **111**, 691–706.

Okal, E.A., 1988. Seismic parameters controlling far-field tsunami amplitudes: a review, *Nat. Haz.*, **1**, 67–96.

Okal, E.A., 2003. Normal modes energetics for far-field tsunamis generated by dislocations and landslides, *Pure Appl. Geophys.*, **160**, 2189–2221.

Okal, E.A., 2007. Seismic records of the 2004 Sumatra and other tsunamis: a quantitative study, *Pure Appl. Geophys.*, **164**, 325–353.

Okal, E.A., 2008. The excitation of tsunamis by earthquakes, in *The Sea: Ideas and Observations on Progress in the Study of the Seas*, Vol. 15, eds. Bernard, E.N. & Robinson, A.R., in press.

Okal, E.A. & Newman, A.V., 2001. Tsunami earthquakes: the quest for a regional signal, *Phys. Earth planet. Inter.*, **124**, 45–70.

Okal, E.A. & Stein, S., 1987. The 1942 Southwest Indian Ocean Ridge Earthquake: largest ever recorded on an oceanic transform, *Geophys. Res. Letts.*, **14**, 147–150.

Okal, E.A. & Synolakis, C.E., 2004. Source discriminants for near-field tsunamis, *Geophys. J. Int.*, **158**, 899–912.

Okal, E.A. & Talandier, J., 1989. M_m: a variable period mantle magnitude, *J. geophys. Res.*, **94**, 4169–4193.

Okal, E.A., Borrero, J.C. & Synolakis, C.E., 2006a. Evaluation of tsunami risk from regional earthquakes at Pisco, Peru, *Bull. seism. Soc. Amer.*, **96**, 1634–1648.

Okal, E.A., Fritz, H.M., Raad, P.E., Synolakis, C.E., Al-Shijbi, Y. & Al-Saifi, M., 2006b. Oman field survey after the December 2004 Indian Ocean tsunami, *Earthq. Spectra*, **22**, S203–S218.

Okal, E.A., Fritz, H.M., Raveloson, R., Joelson, G., Pančošková, P. & Rambolamanana, G., 2006c. Madagascar field survey after the December 2004 Indian Ocean tsunami, *Earthq. Spectra*, **22**, S263–S283.

Oldham, R.D., 1893. *A manual of the geology of India: stratigraphical and structural geology*, Off. Superint. Gov. Printer, Calcutta, 543pp.

Okal, E.A. & Talandier, J., 1991. Single-station estimates of the seismic moment of the 1960 Chilean and 1964 Alaskan earthquakes, using the mantle magnitude M_m, *Pure Appl. Geophys.*, **136**, 103–126.

Ortíz, M. & Bilham, R., 2003. Source area and rupture parameters of the 31 December 1881 $M_w = 7.9$ Car Nicobar earthquake estimated from tsunamis recorded in the Bay of Bengal, *J. geophys. Res.*, **108**(B4), ESE_11, 16pp.

Parsons, T., Toda, S., Stein, R.S., Barka, A. & Dieterich, J.H., 2000. Heightened odds of large earthquakes near Istanbul: an interaction-based probability calculation, *Science*, **288**, 661–665.

Peirce, J.W., 1978. The northward motion of India since the Late Cretaceous, *Geophys. J. Roy. Astr. Soc.*, **52**, 277–312.

Polet, J. & Kanamori, H., 2000. Shallow subduction zone earthquakes and their tsunamigenic potential, *Geophys. J. Int.*, **142**, 684–702.

Quittmeyer, R.C. & Jacob, K.H., 1979. Historical and modern seismicity of Pakistan, Äfghanistan, northwestern India, and southeastern Iran, *Bull. seism. Soc. Am.*, **69**, 773–823.

Ruff, L.J. & Kanamori, H., 1980. Seismicity and the subduction process, *Phys. Earth planet. Int.*, **23**, 240–252.

Satake, S., Shimazaki, K., Tsuji, Y. & Ueda, K., 1996. Time and size of a giant earthquake in Cascadia inferred from Japanese tsunami records of January, 1700, *Nature*, **379**, 246–249.

Satake, K. *et al.*, 2006. Search for evidence of past earthquakes similar to the 2004 event: Paleoseismological Surveys in Andaman Islands and Rakhine Coast of Myanmar, *Eos, Trans. Amer. Geophys. Un.*, **87**(52), U52A-06 [Abstract].

Scharroo, R., Smith, W.H.F., Titov, V.V. & Arcas, D., 2005. Observing the Indian Ocean tsunami with satellite altimetry, *Geophys. Abstr.*, **7**, 230 [Abstract].

Sclater, J.G. & Fisher, R.L., 1974. The evolution of the Eastcentral Indian Ocean, with emphasis of the tectonic setting of the Ninetyeast Ridge, *Geol. Soc. Amer. Bull.*, **85**, 683–702.

Silver, E.A., 1972. Pleistocene tectonic accretion of the continental slope off Washington, *Mar. Geol.*, **13**, 239–249.

Socquet, A., Vigny, C., Chamot-Rooke, N., Simons, W., Rangin, C. & Ambrosius, B., 2006. India and Sunda plates motion and deformation along their boundary in Myanmar determined by GPS, *J. geophys. Res.*, **111**(5), B05406, 11pp.

Solov'ev, S.L. & Go, Ch.N., 1984. Catalogue of tsunamis on the Western Shore of the Pacific Ocean, *Can. Transl. Fish. Aquat. Sci.*, **6077**, 437pp.

Solov'ev, S.L., Go, Ch.N. & Kim, Kh.S., 1986. *Katalog tsunami v tikhom okeane, 1969–1982 gg.*, Akad. Nauk SSSR, Moskva, 164 pp.

Stein, S. & Okal, E.A., 1978. Seismicity and tectonics of the Ninetyeast Ridge area: evidence for internal deformation of the Indian plate, *J. geophys. Res.*, **83**, 2233–2245.

Stein, S. & Okal, E.A., 2005. Size and speed of the Sumatra earthquake, *Nature*, **434**, 581–582.

Stein, S. & Okal, E.A., 2007. Ultra-long period seismic study of the December 2004 Indian Ocean earthquake and implications for regional tectonics and the subduction process, *Bull. seism. Soc. Amer.*, **97**, S279–S295.

Stein, R.S., Barka, A.A. & Dieterich, J.H., 1997. Progressive failure on the North Anatolian fault since 1939 by earthquake stress triggering, *Geophys. J. Int.*, **128**, 594–604.

Synolakis, C.E., 1991. Green's law and the evolution of solitary waves, *Phys. Fluids A*, **3**, 490–491.

Synolakis, C.E., 2002. Tsunami and seiche, in *Earthquake Engineering Handbook*, pp. 9_1–9_90, eds Chen, W.-F. & Scawthron, C., CRC Press, Boca Raton.

Synolakis, C.E. & Kong, L., 2006. Runup measurements of the December 2004 Indian Ocean tsunami, *Earthq. Spectra*, **22**, S67–S92.

Synolakis, C., Imamura, F., Tsuji, Y., Matsutomi, H., Tinti, S., Cook, B., Chandra, Y.P. & Usman, M., 1995. Damage, conditions of East Java tsunami of 1994 analyzed, *Eos. Trans. Amer. Geophys. Un.*, **76**, 257, 261–262.

Tadepalli, S. & Synolakis, C.E., 1996. Model for the leading waves of tsunamis, *Phys. Rev. Letts.*, **77**, 2141–2145.

Titov, V.V. & Synolakis, C.E., 1998. Numerical modeling of tidal wave runup, *J. Waterw. Port, Coastal Ocean Eng.*, **124**, 157–171.

Titov, V.V., Rabinovich, A.B., Mofjeld, H.O., Thomson, R.E. & González, F.I., 2005. The global reach of the 26 December 2004 Sumatra tsunami, *Science*, **309**, 2045–2048.

Tsai, V.C., Nettles, M., Ekström, G. & Dziewoński, A.M., 2005. Multiple CMT source analysis of the 2004 Sumatra earthquake, *Geophys. Res. Letts.*, **32**(17), L17304, 4pp.

Tsuji, Y. *et al.*, 1995. Field survey of the East Java earthquake and tsunami of June 3, 1994, *Pure Appl. Geophys.*, **144**, 839–854.

Viera, V.M., Le Bohec, C., Côté, S.D. & Groscolas, R., 2006. Massive breeding failures following a tsunami in a colonial seabird, *Polar Biol.*, **29**, 713–716.

Vigny, C. *et al.,* 2003. Present-day crustal deformation around the Sagaing fault, Myanmar, *J. geophys. Res.*, **108**(B11), ETG_6, 2533, 10pp.

Visser, S.W., 1922. Vulkanische verschijnselen en aardbevingen in den Oost-Indischen archipel waargenomen gedurende het jaar 1921, *Natuurkunding Tijdschrift voor Nederlandisch Indie*, **82**, 222–269.

Ward, S.N., 1980. Relationship of tsunami generation and an earthquake source, *J. Phys. Earth*, **28**, 441–474.

Weiss, R. & Bahlburg, H., 2006. The coast of Kenya field survey after the December 2004 Indian Ocean tsunami, *Earthq. Spectra*, **22**, S235–S240.

Wessel, P.W. & Smith, H.F., 1991. Free software helps map and display data, *Eos. Trans. Amer. Geophys. Un.*, **72,** 441 and 445–446.

White, R.S. & Klitgord, K., 1976. Sediment deformation and plate tectonics in the Gulf of Oman, *Earth planet. Sci. Letts.*, **32**, 199–209.

Wichmann, A., 1918. Die Erdbeben des Indischen Archipels bis zum Jahre 1857, *Verhandelingen K. Akad. Wetensch. te Amsterdam, Tweede Sectie*, **20**(4), 193pp.

Wiens, D.A., Stein, S., DeMets, D.C., Gordon, R.G. & Stein, C.A., 1986. Plate tectonics models for Indian Ocean 'intraplate' deformation, *Tectonophysics*, **132**, 37–48.

Woods, M.T. & Okal, E.A., 1987. Effect of variable bathymetry on the amplitude of teleseismic tsunamis: a ray-tracing experiment, *Geophys. Res. Letts.*, **14**, 765–768.

Wysession, M.E., Okal, E.A. & Miller, K.L., 1991. Intraplate seismicity of the Pacific Basin, 1913–1988, *Pure Appl. Geophys.*, **135**, 261–359.

Zachariasen, J., Sieh, K., Taylor, F.W., Edwards, R.L. & Hantoro, W.S., 1999. Submergence and uplift associated with the giant 1833 Sumatran subduction earthquake: evidence from coral microatolls, *J. geophys. Res.*, **104**, 895–919.

APPENDIX A: THE 2007 BENGKULU EARTHQUAKES

As this paper was going to press, the occurrence of a major earthquake offshore of Bengkulu, southern Sumatra on 2007 September 12 changes significantly the framework of seismicity in the area of the 1833 rupture, and warrants an updated discussion.

The epicentre of the Bengkulu earthquake was located by the National Earthquake Information Center at (4.52°S; 101.37°E), and thus inside the 1833 fault area, as defined by Zachariasen *et al.* (1999) (Event I on Fig. A1). In this respect this earthquake fits the concept of triggering by Coulomb stress transfer. However, its moment of 5.1×10^{28} dyn × cm makes it much smaller than the 1833 event, of which it clearly cannot be a simple repeat. The earthquake generated a moderate tsunami, with a maximum local run-up of 4 m at Lais, 40 km NW of Bengkulu (Borrero *et al.* 2007), and no damaging effects in the far field. The main shock (Event I, at 11:10 UTC) was followed by a large aftershock ($M_0 = 7.8 \times 10^{27}$ dyn × cm) at the bottom of its rupture zone (Event II, at 23:49) and by a still smaller event under the island of Sipura, probably outside the zone of rupture of the main shock (Event III at 03:35, September 13); this last shock occurred at the location of a cluster of activity during the last quarter of 2005, whose total seismic moment release remained moderate (2.4×10^{26} dyn × cm).

The distribution of aftershocks of the 2007 main shock is compatible with a rupture area of 200 km × 100 km, which would translate into a slip of 5 m. This model agrees with the distribution of aftershocks, with the results of preliminary source tomography (C. Ji, personal communication 2007), and successfully predicts run-up heights surveyed along the coast (Borrero *et al.* 2007).

The plate kinematics models of Chamot-Rooke & Le Pichon (1999) and Socquet *et al.* (2006) predict a convergence rate of 51 mm yr^{-1} between the Sunda and Australian blocks, amounting to an accumulation of 8.9 m since 1833, which the 2007 earthquake

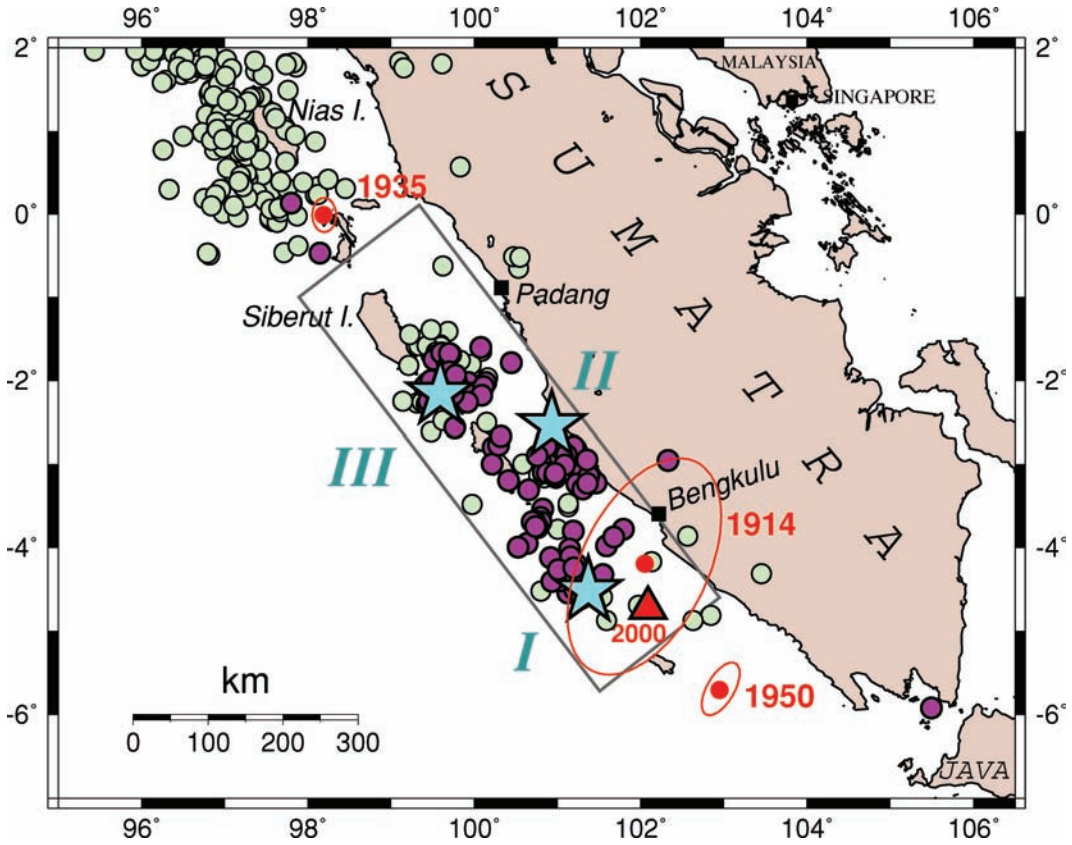

Figure A1. Map of the epicentral area of the 2007 Bengkulu series. The grey rectangle is the fault zone of the 1833 event, as inferred by Zachariasen *et al.* (1999). The three large stars are the epicentres of the 2007 September 12 main shock (11:10 UTC; I), of its main after shock at 23:49 UTC (II), and of the third large event at 03:35 on September 13. The purple dots show the PDE locations of their aftershocks, up to 2007 September 29. Global CMT solutions posterior to the 2004 Sumatra–Andaman earthquake are shown as light green dots. Relocated historical earthquakes are shown as solid red dots with associated Monte Carlo ellipses. The triangle identifies the 2000 earthquake.

has, therefore, not fully released. We also note (Fig. A1) that the aftershock zone of the Bengkulu earthquake fails to cover the entire 1833 rupture area, even taking into account Event III, whose low moment ($M_0 = 4.4 \times 10^{26}$ dyn $\times$ cm) makes it a negligible contributor to the plate convergence budget. As for the earthquake of 04 June 2000 (4.73°S; 101.94°E; $M_0 = 7.5 \times 10^{27}$ dyn $\times$ cm), its aftershocks extend 170 km to the southeast, suggesting that it did not affect the 1833 rupture area. Finally, we note that Newcomb & McCann (1987) list an earthquake on 1914 June 25, assigned $M = 7.6$ by Gutenberg & Richter (1954), but not listed in the NEIC database. Its isoseismals would suggest a location at sea, although no records of a tsunami are mentioned in Solov'ev & Go's (1984) authoritative catalogue. We relocated this earthquake, using the technique of Wysession *et al.* (1991), to (4.19°S; 102.03°E), with the Bengkulu epicentre only 82 km away and inside its Monte Carlo ellipse (computed with $\sigma_G = 10$ s, appropriate for 1914). The true size of the 1914 event and its possible contribution to tectonic strain release can only be speculated, pending a quantitative assessment of its source, based on historical seismograms.

To the north of the 1833 earthquake, a large event occurred on 1935 December 28 with a magnitude $M = 8.1$ assigned at Pasadena by Gutenberg & Richter (1954). Its epicentre is remarkably well constrained, relocating at (0.01°S; 98.19°E), with its Monte Carlo ellipse remaining outside the 1833 fault area (Fig. A1).

The preliminary picture emerging from the occurrence of the 2007 event(s) is that there remains strain accumulated since the 1833 event along its fault area. Note the seismic gap between ~0.5°S and 2°S; furthermore, the seismic slip released in 2005–2007 between 2°S and 5°S does not account for the accumulated convergence, especially in the area of the 2005 cluster and Event III. In the area of rupture of Event I, this deficiency is less flagrant, and could even be absent, if the 1914 event turned out to be comparable in rupture area and size to Event I, a scenario improbable on account of the absence of tsunami reports, but which cannot be totally dismissed.

In the framework of basin-wide tsunami risk, the major question remains at present the possibility, in the next few years to decades, of either a repeat of the 1833 event under Scenario 1, or the rupture of a fault extending to the south under Scenario 2. While either scenario would entice rupturing through the fault area of the 2007 Bengkulu earthquake, we have argued above for remanence of strain accumulated since 1833, and we further note that a similar process took place during the 2004 Sumatra–Andaman earthquake, whose rupture extended over and beyond the fault area of the 1881 Car-Nicobar earthquake (Ortíz & Bilham 2003). At $M_0 = 7 \times 10^{27}$ dyn $\times$ cm, the latter was smaller than the 2007 Bengkulu event, but it also occurred in a zone featuring a lesser convergence rate. Most source tomography models of the 2004 event identify the 1881 fault zone (from 8.5°N to 9.7°N) as an area of reduced, but not vanishing, slip and moment release (Ishii *et al.* 2005; Banerjee *et al.* 2007; Chlieh *et al.* 2007); it certainly did not play the role of a barrier, since the 2004 rupture effectively 'jumped' it and extended all the way to 14.5°N. Several similar examples are documented in the Central and South Peru subduction zones, which also host

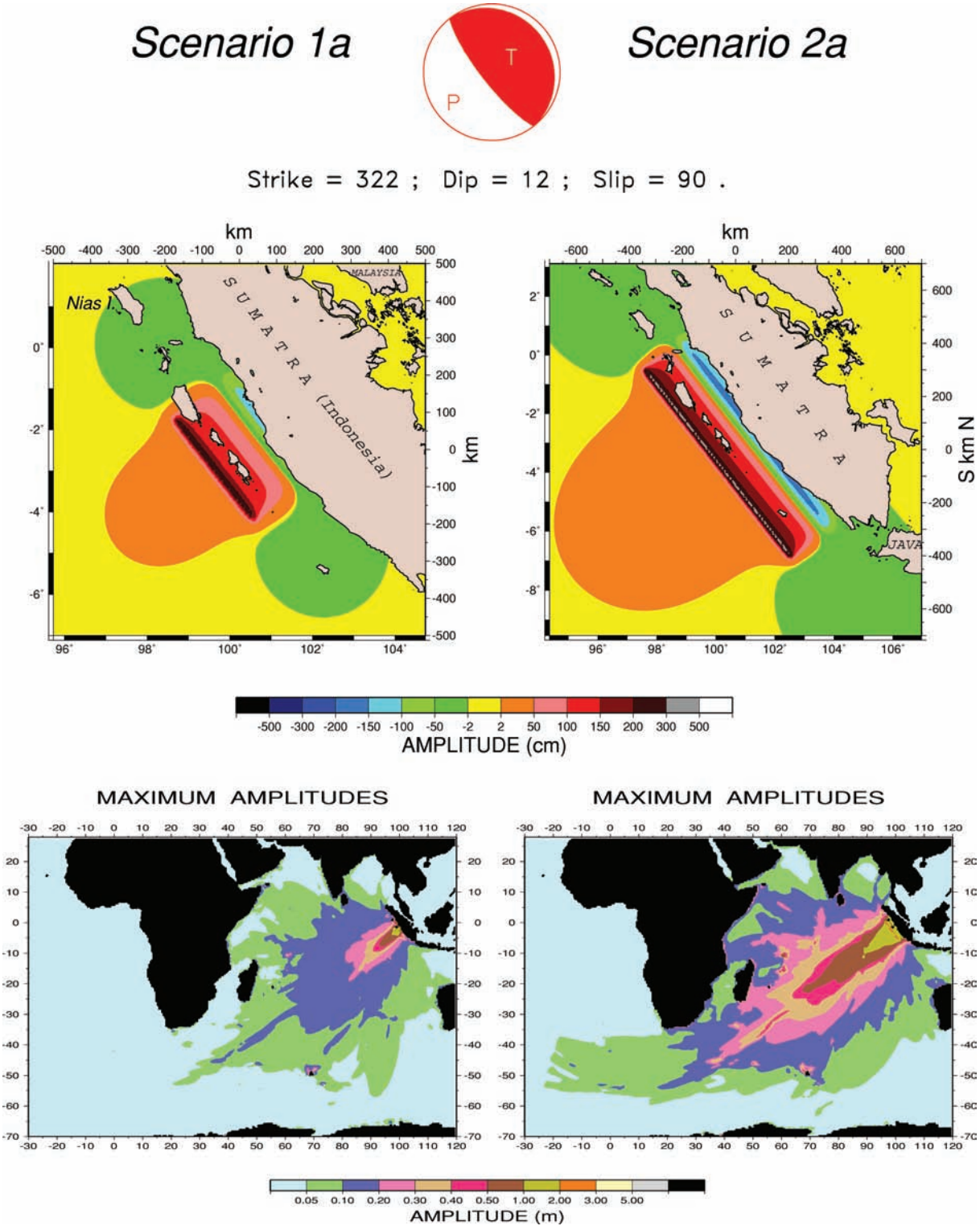

Figure A2. Same as Fig. 4 for the modified Scenarios 1a (left-hand panel) and 2a (right-hand panel).

mega-earthquakes (Dorbath *et al.* 1990); for example, the catastrophic 1687 rupture off Pisco overrode the fault zone of the smaller 1664 event, the latter large enough to have generated a destructive local tsunami (Okal *et al.* 2006a).

It is of course impossible to predict exactly where, and especially how big, will be the next episode of major strain release along the southern Sumatra subduction zone. The occurrence of the Bengkulu earthquake has probably lessened the likelihood of Scenarios 1 or 2, but they remain feasible models for mega earthquakes in the area. In particular, Scenario 1 is known to have occurred in 1833, and thus will recur at some point in time.

We complement these case studies by new simulations shown on Fig. A2: Scenario 1a is adapted from Scenario 1 by reducing the size of the source ($L = 350$ km; $W = 175$ km; $\Delta u = 6$ m;

$M_0 = 1.7 \times 10^{29}$ dyn $\times$ cm) and keeping it within the fault area of the 1833 earthquake; it represents a major event possibly releasing the remainder, after 2007, of the strain accumulated there since 1833. Scenario 2a is a long fault inspired from Scenario 2, but with an average slip reduced to 8 m ($M_0 = 6 \times 10^{29}$ dyn $\times$ cm), to take into account the partial strain release in its northern segment during the 2007 Bengkulu event.

Fig. A2 shows that, as expected, the amplitudes of the resulting far-field tsunamis are reduced; Scenario 1a yields deep-water amplitudes in the western Indian Ocean generally comparable to those of 2004, plotted on Fig. 2(e) (with the exception of Somalia), and, therefore, poses significant hazard. As for Scenario 2a, it gives results remarkably similar to those of the original Scenario 1, which further illustrates the primordial role of seismic moment (shared by the two events) in controlling far-field tsunami amplitudes, as discussed in Section 3.

In conclusion, far field tsunami hazard from South Sumatra subsists in the Indian Ocean Basin despite the occurrence of the Bengkulu earthquake. However, we re-emphasize that Scenarios 1, 2, 1a, 2a represent plausible future tsunamis, but not necessarily the next one[s] to originate at the South Sumatra coastline.